Liquid Jet Interaction with a Moving Surface

by

PURUSHOTAM KUMAR

B.Tech Indian Institute of Technology Guwahati, INDIA, 2009

A THESIS SUBMITTED IN PARTIAL FULFILLMENT OF THE REQUIREMENTS FOR THE DEGREE OF

MASTER OF APPLIED SCIENCE

in

THE FACULTY OF GRADUATE STUDIES

(Mechanical Engineering)

THE UNIVERSITY OF BRITISH COLUMBIA
(Vancouver)

August, 2011

Abstract

An experimental study was conducted to study the splash-deposition characteristics of a liquid jet impinging on a moving surface. The main focus of this study was to determine the effects of fluid, flow and surface properties on the outcome of the jet impingement. Several parameters such fluid viscosity, elasticity and surface tension, jet and surface velocity, jet diameter surface wettability and surface roughness were changed and their effects on splash-deposition characteristics were analyzed during this research work.

For non-Newtonian fluids increase in the yield stress and consistency constant of the fluids helps in inhibition of the splash. At high Weber number the effects of surface tension and jet impingement angle were negligible compared to effects of Reynolds and Oldroyd numbers. But at smaller Weber number effects of surface tension were comparable to that of Reynolds number. It was also observed that the both normal (jet velocity) and tangential (surface speed) speeds play roles in splash-deposition dynamics.

Newtonian liquid jet with smaller diameter illustrated that effect of surface tension becomes prominent only for liquids with low viscosities and for these liquids and 200 micron nozzle jets deposit up to 40 m/s. For high viscosity liquid same trend of deposition was observed and jets deposit up to 35 m/s. It was also observed that the jets of smaller viscosities spread on the surface very easily, making few micron sized lamella. Although higher viscosities liquid jets still spread very easily on the surface, the lamella thickness was much larger than that of low viscosity liquids. It was also found that mid-range viscosities jet started to splash at much lower velocities (13 m/s). This behavior is related to balancing of inertia forces by both the surface tension and viscous forces.

Preface

The authors of chapter 2 are Purushotam Kumar, Sheldon Green, Don Eadie. Dr. Green identified the need for further information regarding yield stress and shear thinning liquid jet interaction with a moving surface. I determined the research variables to be tested (fluids, jet and surface velocities, and surface properties) and the method for performing these tests with the supervision of Dr. Green. I performed all of the experimental testing for the research. With direction from Dr. Green and Dr. Eadie, I performed data analysis to determine the effects of the research variables and provided conclusions regarding the meaning of the results. I wrote the manuscript with the revisions and suggestions from Dr. Green and Dr. Eadie. A version of this chapter will be submitted for publication. The authors of this paper will be Purushotam Kumar, Sheldon Green and Don Eadie.

The authors of chapter 3 are Purushotam Kumar, Sheldon Green, Don Eadie. Dr. Green identified the need for further information regarding effects of surface tension and jet diameter on splash-deposition characteristics of Newtonian jet. Dr. Eadie identified the possibility of using smaller diameter nozzles to reduce mass flow rate while keeping the jet velocities sufficiently high. I determined the research variables to be tested (nozzle diameter, liquid viscosities and surface tensions, jet/surface velocities), the method for performing these tests and the analysis. I conducted all the experiments for the research. With direction from Dr. Green I performed data analysis to determine the effects of the research variables and provided conclusions regarding the meaning of the results. I wrote the manuscript with revisions and suggestions from Dr. Green and Dr. Eadie. A version of this chapter will be submitted for publication. The authors of this paper will be Purushotam Kumar, Sheldon Green and Don Eadie.

The authors of chapter 4 are Purushotam Kumar, Sheldon Green, Don Eadie, David Elvidge. Dr. Eadie and Dr. Elvidge identified the need for further information regarding combined effects of shear thinning and elasticity on results of a liquid jet impingement on a moving surface. Dr. Green and Dr. Eadie identified the possibility of studying effects of surface temperature on splash threshold for these liquids. I determined the research variables to be tested (jet and surface speeds, nozzle diameters and surface temperature), the method for performing these tests with the supervision of Dr. Green. I performed all of the experimental testing for the research. With direction from Dr. Green and Dr. Eadie, I performed data analysis to determine the effects of the research variables and provided conclusions regarding the meaning of the

results. I wrote the manuscript with the revisions and suggestions from Dr. Green, Dr. Eadie and Dr. Elvidge.

Table of Contents

Abstract ii

Preface iv

Table of Contents vi

List of Tables ix

List of Figures x

List of Symbols xii

Glossary xiv

Acknowledgements xv

Chapter 1 - Introduction 1

1.1 Introduction to friction control in rail road industry 1

1.2 Friction modifiers and modes of applications 1

1.3 Newtonian droplet impact on a stationary and moving surface 2

1.4 Yield stress and shear thinning droplet impact 2

1.5 A Liquid jet impingement on stationary and moving surfaces 3

1.6 Research objectives 5

Chapter 2 - Non-Newtonian Liquid Jet Interaction with a Moving Surface 7

2.1 Introduction 7

2.2 Sample preparations 7

2.3 Rheological properties of the carbopol solution 8

2.3.1 Calculation of yield stress 9

2.4 Apparatus and method 11

2.5 Results and discussion 13

2.5.1 Flow rate measurement 13

2.5.2 Splash – deposition experiment 16

2.6 Summary 21
Chapter 3 - Newtonian Liquid Jet Interactions with a Moving surface 23
3.1 Introduction 23
3.2 Experimental setup and test liquids prepared 23
3.3 Results and discussion 25
3.3.1 Flow rate measurement 25
3.3.2 Spread radius, spread width and lamella thickness 28
3.3.3 Splash – deposition experiments 31
3.4 Mathematical explanation for splash of liquid jets of mid-range viscosities 37
3.4.1 Comparison of forces/stresses on lamella 38
3.5 Summary 40
Chapter 4 - Experiments using KELTRACK® Solutions 42
4.1 Introduction 42
4.2 Liquids prepared 42
4.3 Results and discussions 42
4.3.1 Rheometry of the liquids 42
4.3.2 Mass flow rate measurements 44
4.3.3 Splash-deposition experiments 46
4.4 Summary 49
Chapter 5 - Conclusions and Recommendations for Future Works 50
5.1 Conclusions 50
5.1.1 Conclusions for non-Newtonian fluids 50
5.1.2 Conclusions for Newtonian fluids 51
5.1.3 Conclusions for KELTRACK solutions 51
5.2 Strength and limitation of thesis research 52
5.3 Potential applications of research findings 52
5.4 Recommendations for future works 53

Bibliography 54
Appendices 57
A - Effect of static contact angles 57
A.1 Test liquid and surfaces 57
A.2 Results and discussion 57
A.3 Conclusions 59
B - Experiments with pure shear thinning fluids 60
B.1 Mass flow rate experiments 60
B.2 Splash-deposition results 61

List of Tables

Table 1 Rheological properties of Carbopol solutions 10
Table 2 Rheological properties of water-glycerin mixtures 24
Table 3 Rheological properties of water-propylene glycol mixtures 25
Table 4 Dimensions of three different nozzles 28
Table 5 Spread radius and spread width of water for different jet and surface speeds 29
Table 6 Rheological properties of KELTRACK® solutions 44
Table 7 Rheological properties and splash thresholds of KELTRACK® solutions 48
Table 8 Static contact angles in degrees 57
Table 9 Rheological properties of water-xanthan gum solutions 60
Table 10 Splash thresholds for water-xanthan gum solutions 62

List of Figures

Figure 1 Prediction of the yield stress of the Carbopol solutions using a shear viscosity versus shear rate curve 9
Figure 2 Shear stress versus shear rate curves for different Carbopol solutions 11
Figure 3 Layout of experimental setup 12
Figure 4 Projectile with steel surface attached 12
Figure 5 Light source and high speed camera assembly 12
Figure 6 Mass flow rates of different cabopol solutions 14
Figure 7 Mass flow rates in cavitation and hydraulic flip regions [30] 14
Figure 8 Discharge coefficient of Carbopol solutions with 648micron nozzle 16
Figure 9 A Liquid jet impinging on a moving surface 16
Figure 10 Effects of the Reynolds number and Oldroyd number on splash-deposition results of Carbopol solutions 18
Figure 11 Effects of the Weber number and Reynolds number on splash-deposition results of Carbopol solutions 19
Figure 12 Effects of the jet impingement angle and Reynolds number on splash-deposition results of Carbopol solutions 20
Figure 13 Effect of Bingham number on splash threshold 21
Figure 14 Mass flow rates of water-glycerin solutions through a 200 micron nozzle 25
Figure 15 Discharge coefficient of water-glycerin solutions dispensed through 200 and 648 micron nozzles 26
Figure 16 Nozzle assembly and precision pinhole 27
Figure 17 Geometry and dimension of the precision pinholes 27
Figure 18 Simple representation of a liquid spreading on a moving surface 28
Figure 19 Representation of a jet spreading on a moving surface 30
Figure 20 Impingement of water (left), WG-60 and WG-85 (right) jets (generated from a 200 micron nozzle) with jet speed of 15 m/s on a surface moving from left to right at 5 m/s. 31
Figure 21 Effects of Re and Ca on the splash-deposition results of water-glycerin solutions dispensed through a 200 micron nozzle 32
Figure 22 Effects of Reynolds and Ohnesorge number on the splash-deposition results of water-glycerin solutions dispensed through a 200 micron nozzle 33
Figure 23 Effect of jet impingement angle and Ca on splash-deposition results of water-glycerin solutions dispensed through a 200 micron nozzle 34

Figure 24 Impingement of water (left), WG-75 and WG-85 (right) jets (generated from a 400 micron nozzle) with a jet speed of 15 m/s on a surface moving from left to right at 5 m/s. 35
Figure 25 Effects of Re and Ca on splash-deposition results of water-glycerin solutions using a 400 micron nozzle 35
Figure 26 Effect of the jet impingement angle and Ca on splash-deposition results of water-glycerin solutions using a 400 micron nozzle 36
Figure 27 Impingement of WPG-05 (left), WPG-50 and WPG-75 (right) jets (generated from a 200 micron nozzle) with a jet speed of 15 m/s on a surface moving from left to right at 5 m/s ... 37
Figure 28 Inertial, shear and surface tension stresses on the lamella 39
Figure 29 Total stress on the lamella 40
Figure 30 Storage and Loss moduli of the KELTRACK® Normal Hi-rail solution 43
Figure 31 Shear viscosities of KELTRACK® solutions 44
Figure 32 Mass flow rates of KELTRACK® solutions projected through a 400 micron nozzle ... 45
Figure 33 Jet velocities of KELTRACK® solutions projected through a 400 micron nozzle 45
Figure 34 Jet velocity = 27.4, surface velocity = 10.1 m/s 46
Figure 35 Jet velocity = 29.7, projectile velocity = 10.5 m/s 47
Figure 36 Jet velocity = 26.9, projectile velocity = 6.77 m/s at 55°C surface temperature 48
Figure 37 (A-C) Deposition and (D-E) splash of an elastic jet on a moving surface traveling from left to right with 5.3 m/s. Jet speed in left column (A-C) is 11.3 m/s, before splash threshold and in right column (D-F) is 13.5 m/s, after splash threshold. 58
Figure 38 Mass flow rates of water-xanthan gum solutions 61

List of Symbols

D	Diameter [m]
H	Thickness of nozzle [micron]
r	Radius [m]
R	Radius [m]
V_J	Jet velocity or normal velocity [$m.s^{-1}$]
V_S	Surface velocity or tangential velocity [$m.s^{-1}$]
V_{rel}	Relative velocity [$m.s^{-1}$]
Ca	Capillary number
Re	Reynolds number
We	Weber number
Od	Oldroyd number
Bi	Bingham number
α	Jet impingement angle in target surface frame of reference [degree]
σ	Surface tension [$N.m^{-1}$]
ε	Surface roughness height [m]
μ	Dynamic viscosity [Pa.s]
ρ	Density [$kg.m^{-3}$]
Wt	Weight
Cd	Discharge coefficient
$\dot{m}$	Mass flow rate [$kg.s^{-1}$]
T	Lamella thickness [m]

k	Consistency constant
n	Power law index
τ	shear stress [Pa]
τ_0	Yield stress [Pa]
ΔP	Nozzle pressure [pa]
D_{Jet}	Jet diameter [m]
X	Spread radius or radius of lamella [micron]
W	Spread width [micron]

Glossary

Splash Threshold – This is defined as the maximum resultant velocity at which deposition is possible on a target surface. This includes both jet and surface velocity.

Critical Reynolds Number – This is defined as minimum Reynolds number which no deposition is possible. This Reynolds is calculated based on liquid jet relative velocity and jet diameter.

Lamella Thickness - This is thickness of liquid spreading on the surface. This thickness is very small closer to impingement point and it increases with increase in the distance from impingement point. For this lamella thickness is taken as average thickness from impingement point to radius at which liquid comes to stop.

Jet Diameter - This is defined as diameter of the liquid jet very close to the target surface. The value of jet diameter varies with liquid velocity and viscosity. It is not same as nozzle diameter because of contraction of expansion of the liquid jets.

Acknowledgements

I extend my sincere gratitude to my supervisor Dr. Sheldon Green who provided unending guidance in my research. I thank him for providing critical insight into the research problems and for allowing me the freedom to investigate solutions in my own manner. I also thank him for challenging me to set the benchmark ever higher and for his support throughout this project. It was a pleasure working with you.

I would like to gratefully acknowledge Dr. Don T Eadie and Dr. David Elvidge of Kelsan Technologies Corporation for their assistance in defining the research objectives and their patience in explaining relevant concepts that were outside of my field of expertise.

I would like to thank the technicians without whose help I could not have completed this study. Thanks to George Soong of the UBC Pulp and Paper Centre and Vishnu Charan Sangem of the Materials Engineering Microscopy Lab.

I would like to thank the Natural Science and Engineering Research Council of Canada (NSERC) and Kelsan Technologies Corporation for their financial support of this project.

I would like to thank Dr. Jimmy Feng, Dr. Ian Frigaard, Bavand Keshavarz, Sarah Hamrozi, Nader Naroozi and Eva Lillqvist for their helpful suggestions and discussion during this project.

Finally, I would like to thank the members of my research group for their continued comments and suggestions concerning explanations and reasoning of experimental outcomes and their friendship throughout the past two years.

Chapter 1 - Introduction

1.1 Introduction to friction control in rail road industry

The Canadian railway network, comprised of more than 72,000 kilometers of track through five time zones [1], annually transports more than 270 million tons of freight. Rail transport is one of the most efficient and cost-effective forms of freight transportation in North America. With rising fuel costs making truck and air transport less efficient and with a continuing increase in population, railways will continue to increase their influence.

Due to this continuing economic influence, ongoing research is being followed by the industry into further improving the efficiency of rail transport. Railroads have recognized that by using an integrated approach to effectively managing the wheel-rail interface, significant benefits such as controlling wheel and rail wear and reducing fuel costs, can be obtained [33]. Recently, researchers have begun to focus their efforts on top of rail (TOR) friction control.

Although it was discovered that TOR friction control significantly reduced fuel consumption [34], this is still a relatively new field as most of the world's railway industries still operate today without TOR friction management.

1.2 Friction modifiers and modes of applications

Friction modifiers exist either as solid sticks or as water-based solutions, with the latter denoted as liquid friction modifiers (LFM's), which contain suspended polymeric and solid composites [34]. By introducing these suspended solids with engineered frictional properties in appropriate quantities into the wheel/rail interface, the frictional characteristics of the layer between the wheel/rail interface, containing wear debris and contaminants, can be modified accordingly [35]. FM's are able to reduce, control, and maintain frictional levels at a specified optimal level over a given number of wheel/train passes, a significant advantage over hydrocarbon based lubricants [34].

Kelsan Technologies Corporation, located in North Vancouver, BC, is a leader in developing friction modifiers for the railway industry. They have developed a number of FM's for use in various applications where differing friction characteristics are required. Of particular interest, is a high positive friction LFM known as KELTRACK HI-RAIL. Due to the compositional nature of this friction modifier, it inherently exhibits non- Newtonian behavior. KELTRACK HI-RAIL will be

discussed further in Chapter 4. The LFM that has been studied by the authors is a water-based suspension of polymers and inorganic solids with non-Newtonian characteristics [1,2].

Currently, air-blast atomizers are used to transfer FM liquids (in the form of ligaments and droplets) to rail surfaces. The associated transfer efficiency is poor, however, due to irregularities in droplet shape and size [3]. As well, when in the presence of a cross wind, LFM droplets can splash or miss the track entirely [3]. For effective deposition on a rail, the droplets/ligaments must move at a velocity high enough to avoid excessive deflection in a crosswind, but low enough to avoid splash or rebound following impaction. Excessive deflection and splash significantly reduces transfer efficiency [4,5].

1.3 Newtonian droplet impact on a stationary and moving surface

Droplet impact and spreading has received attention for a variety of technical applications such as thin film coating, pesticide application, spray painting, spray combustion, spray cooling of hot surfaces, deposition of solder bumps on printed circuit boards and inkjet printing. The phenomenon is also relevant to the coating quality and process performance for air-suspension coating of food powders, although no direct study has been related. Studies carried out by several authors [6-8] reveal that the splash or deposition of a droplet upon impingement depends on several parameters including viscosity, density and surface tension. Other authors have studied the impact of Newtonian droplets on a moving surface, and conclude that both the normal and tangential speed of the drop (in the reference frame of the surface) affect splash. For a droplet impacting on a moving surface Bird et al. [9] reported that based on the magnitude of the tangential velocity, there are three behaviors: the lamella will spread in all directions, splash in all directions, or splash asymmetrically. They further concluded that when there is no tangential velocity, the drops either spread or splash in all directions. When the symmetry is broken through the tangential velocity however, the transition bifurcates and causes a new behavior: asymmetric splashing.

1.4 Yield stress and shear thinning droplet impact

Studying the yield stress liquid droplets, Nigen [10] reported that when projected at low-impact velocities, droplets first behave like deformable solids. A long time scale creeping flow then follows. When projected at high-impact velocities, the droplet velocity and stress decreases as the droplet spreads, eventually falling below the yield value. When the limit is reached, the spreading of droplet stops immediately. The impact morphology of drops comprised of shear-thinning fluids [11] was qualitatively similar to that of Newtonian fluids, but viscoplastic drops showed central drop peaks at the end of inertial spreading.

German and Bertola [11] further reported that both the yield stress and viscosity of the viscoplastic fluids inhibit the spreading of the lamella on the surface. In cases of capillary-driven spreading of yield stress drops [12], the spreading rate is affected both by the degree of fluid shear thinning and the yield stress magnitude. The Bingham-Capillary number is a dominant parameter for viscoplastic liquids. For fluids with a Bingham–Capillary number below unity (which includes shear thinning, Newtonian and low yield-stress magnitude fluids), the static contact angle remains constant, irrespective of the yield-stress magnitude or impact conditions. For fluids with a Bingham–Capillary number greater than unity however, the static contact angle varies depending on both the yield-stress magnitude and the impact conditions. In an experimental study conducted by Saidi et al. [13], it was shown that increasing the yield stress dictates the drop formation, while also inhibiting spreading and weakening retraction in the case of high inertial impacts.

1.5 A Liquid jet impingement on stationary and moving surfaces

Though experimental, analytical and numerical studies have provided numerous data on free impinging jets, submerged jets and confined jets, data are most often only concerned with the heat transfer capabilities of free or submerged impinging jets. In the presence of a moving plate surface, jet impingement involves a much more complicated flow structure. Since the amount of liquid adhering to the moving surface depends on the nature of the flow field, a full understanding of the flow structure is necessary to understand the stability of the liquid sheet on the surface.

Previous studies provide valuable results on free surface impinging jet behavior. The theory of film flows is thoroughly described in the precursor works of Watson [14]. Using boundary layer theory, Watson analytically measures the expression of velocity fields for the four flow regions [14]. Watson divides the flow radially into a stagnation region, a boundary layer region with a surface velocity equal to the jet velocity, a region of decreasing free surface velocity, and, finally, a hydraulic jump, and expresses the solution in a self-similar manner. In the experiments conducted by Nakoryakov et al. [15], Watson's analytical results were discussed further. Using laser-Doppler measurements, Azuma and Hoshino [16] experimentally verified Watson's expressions for the laminar boundary layer, similarity region and film thickness. Stevens and Webb's [17] analytical predictions compare velocity profile (LDV), layer depth and free surface velocity measurements. They show that the maximum velocity of the layer is not at the free surface for $r/d < 2.5$, in effect invalidating assumptions held by many analytical models focusing on this flow region. Over the last three to four decades film flows have thus been studied widely, velocity fields of each region have been determined, and these results can be applied to further studies on convective heat transfer problems [17-19]. Bohr et al. [20] show that the radius of the jump depends on the volume flow rate and kinematic viscosity, with g as the gravitational acceleration.

Despite the significant practical importance and ample existing research on rolled metal cooling, jet impingement on moving surfaces has received far less attention. Zumbrunnen et al. [21,22] reveal that

the presence of a moving surface strongly influences both the flow field and the heat transfer efficiency for plane jet impingement. Their results show that water dispensed from the nozzle divides upon impaction with a plate (moving or not); the flow direction can run either with or opposite to the direction of plate motion. The moving plate can facilitate the transport of fluid away from the stagnation line. However, on the other side of the stagnation line, the fluid becomes entrained and is at risk of penetrating the impingement region beneath the jet again. Although the flow structure of an axisymmetric water jet impinging a moving plate is much more complicated because the jet divides in all directions, the same phenomena of fluid re-entrainment occurs. Zumbrunnen [21] solved the Navier–Stokes equations through similarity analysis; the heat and mass transfer distributions were determined by numerically solving the conservation equations for energy and species. He concluded that the effect of the surface motion on fluid flow is confined to a thin region, which can be represented by the velocity boundary layer thickness for a plane jet impinging on a stationary surface. Convective heat transfer remains unaffected by the surface motion when the surface temperature is constant along the impingement surface. However, in the case of a spatially dependent temperature, convective heat transfer is dependent on the dimensionless surface velocity VS. In most applications using impinging jets, surface temperature decreases in the direction of surface motion. Using a large eddy simulation technique, Chattopadhyay and Saha [23] numerically study the flow field for rectangular, submerged jet impingement on a moving surface for a moderately high Reynolds number (Re = 5800). They provide a large database of turbulent quantities for such a configuration.

Although Hydraulic jumps are different phenomena from jet impingement on a moving surface, the fluid pattern near the impingement point will still be useful for this study. The fluid viscosity acts to hasten the diffusion of vorticity across the fluid layer, decelerating the flow [24]. This decreases the jump radius and increases the height of the jump. Gradeck et al. [25] reported that for hydraulic jump on a moving surface, the jump radius and jump height depend on the volume flow rate, kinematic viscosity and gravitational acceleration. They [25] also derived a power relation for calculating the radius of the jump, in which the Reynolds and Weber number emerged as main variables. Roisman et al. [26] have shown that the mechanism of splash is related to the bending instability of a rim bounding on a free liquid sheet. The rim instability is caused by the moment of force associated with the inertia of the liquid entering the rim. This type of instability leads to the complete breakup of the crown, and the formation of several finger-like jets based at the wall film. Li et al. [27] categorized sheet breakup regimes as Capillary instability and Kelvin-Helmholtz instability regimes. They have shown that a liquid sheet starts to breakup due to the sheet's superposition with aerodynamic waves. The hydrodynamic wave, generated at the point of impingement, also causes sheet instabilities.

In a recent work, Keshavarz [28] reported on the impingement of a Newtonian jet on a moving surface. They concluded that viscous effects are more important than surface tension in determining splash. They

also showed that the Reynolds number and surface roughness are more important parameters than the Weber number and impaction angle in determining jet impingement results.

1.6 Research objectives

The Liquid Friction Modifiers are very effective product in reduction of friction between rail track and the wheel but current application or delivery method is not very effective. The effectiveness of the product method is defined as the percentage of the sprayed product that adheres to the rail surface. This value is called the transfer efficiency. The primary objective of this research work is to achieve best possible transfer efficiency while providing a uniform deposition on the target surface. Thus it is necessary to understand the liquid jet interaction with the moving surface. The Liquid friction modifiers are non-Newtonian liquids with small yield stress, strong shear thinning, reasonable elasticity. Therefore analyzing each component of this product is also important.

The first objective of this research work was to determine the effects that liquid jet and projectile speed have on the outcome of the jet impingement on a moving surface. The second objective was to analyze the roles of individual fluid properties such as surface tension, shear viscosity and elasticity on the jet impingement. The combined effects of both shear thinning and elasticity or yield stress were also a major concern during this study. Another objective of this research work was to understand the effects of the jet diameter and height between nozzle and the target surface.

These research objectives were achieved by studying the interaction of a Newtonian and non-Newtonian liquid jet with a moving surface. Several Newtonian liquids such as water-glycerin and water-propylene glycol solutions and non-Newtonian liquids such as water-Carbopol and water-xanthan gum solution were prepared.

In Chapter 2 the effects of the yield stress, shear thinning and power-law index on behavior of jet impingement and splash dynamics are investigated. Preparation of yield stress fluids along with calculation of yield stress of Hurchel-bulkley type fluids are also discussed in this chapter. Finally effects of dimensionless numbers such as Reynolds, Weber and Oldroyd numbers are investigated.

In Chapter 3 the effects of nozzle diameter, jet and surface speed, surface tension and viscosity are investigated. It also discusses the lamella thickness and spread width of the liquids on the surface. The dominance of the surface tension forces over the viscous forces is also investigated in this chapter. Finally a qualitative mathematical explanation has been provided for the experimental results obtained.

Chapter 4 has been devoted to results obtained from actual liquid friction modifiers experimentations. This chapter gives detailed results about the rheometry, mass flow rate and splash-deposition experiments with three Keltrack solutions received from Kelsan Technologies Corporation. It also investigates the combined effects of strong shear thinning and reasonable elasticity on jet impingement.

Chapter 5 provides conclusions that can be drawn from the above mentioned experimental studies and describes the contributions to knowledge of this work. The chapter closes with recommendations for future work that can be performed using the experimental apparatus used for these investigations.

Chapter 2 - Non-Newtonian Liquid Jet Interaction with a Moving Surface

2.1 Introduction

The behavior of a non-Newtonian liquid jet impinging on a moving surface has been studied experimentally by means of high-speed imaging. In this chapter, we focus on the role of the yields stress and shear thinning properties of liquids, the resultant velocity of the jet and surface, and jet impingement angle, on the splash characteristics of a liquid jet impingement. Seven different non-Newtonian solutions (Carbopol and water solutions) with wide range of yield stress and consistency constant were used to understand the effects of underlying parameters. The jet and surface speed of this experimental study ranges from 5 – 40 and 5 -15 m/s respectively. With these experimental settings we were able to analyze effects of several dimensionless parameters (Reynolds number, Weber number, Oldroyd number and Jet impingement angle).

The experimental results show both jet and surface speeds play roles in splash-deposition behavior of jet impingement. The role of both Reynolds and Oldroyd number were dominant but Weber number was only dominant at low Weber number values. Finally we also observed that the ratio of the jet velocity to surface velocity (Jet impingement angle) was not an important variable compared to resultant jet velocity. With this research work we are to show that the increase in the yield stress and consistency constant of liquids reduce the chances of inhibition.

2.2 Sample preparations

Carbopol® 940 was used to study the effects of yield stress and the consistency constant of a non-Newtonian liquid. Carbopol® 940 is a white, powder-like chemical. When mixed with water it shows a week, acidic behavior with a pH values in range of 3.0 to 4.5 (depending on the concentration of Carbopol in the water). To get a proper gel-like solution of Carbopol, the mixture's pH has to be brought up to levels from 5.5 – 6.0. In this range, the liquid shows both yield stress and shear thinning. The gel-like solution is very stable and does not degrade over a few weeks.

To prepare this solution, we mixed the required amount of Carbopol into distilled water to obtain the desired percentage of Carbopol. The mixture of powdered Carbopol and water was stirred for at least 24 hours using a double impeller stirrer. After several hours of stirring, small bubbles become entrapped in the mixture, which are difficult to remove once the gel has formed.

Therefore, we let the solution rest for 1 – 2 hours, allowing the small bubble to disappear. Later on, several drops of the 30% NaOH solution were added to the Carbopol and water mixture to bring the pH value up to the 5.5 – 6.0 range. The Carbopol-water mixture was stirred continuously while adding the NaOH. To avoid over-addition of NaOH, we simultaneously monitored the pH value while mixing the solution. Once a reasonable gel-like Carbopol solution was obtained, another 24 hours of stirring was done before beginning the rheometry, flow rate and splash-deposition experiments.

2.3 Rheological properties of the carbopol solution

The Carbopol solution shows both yield stress and shear thinning behavior. In other words, at low shear rates it behaves like a solid, but at high shear rates it flows like any other fluids. Carbopol is a long chain polymer and due to its entanglement the chain does not break at lower shear rates therefore the solution shows yield stress but as the shear rate is increased the polymer chains start to align in the direction of flow, and hence it shows shear thinning behavior.

The Carbopol solution is a Hurchel-Bulkley type fluid and its rheological properties were measured using Bohlin CS 10 rheometer. This rheometer allows us to experiment with several methods of measurement assembly such as cones and plates, parallel plates, concentric cylinders and parallel plates with serrated surfaces. Though all of these configurations were used to check the rheometry and results, serrated parallel plates were the most effective. Thus, henceforth we continued to use the serrated parallel plate configuration. We also followed the methods explained by Nguyen and Boger [32] for measuring the rheological properties of the yields stress fluids.

This rheometer uses a built-in computer program that allows users to control the shear rate applied to the sample. The rheometer can apply ramped, linear increasing, linear decreasing and increasing-decreasing shear rates. The increasing-decreasing shear rate is particularly useful in quantifying the memory effect of Carbopol samples.

$$\tau = \tau_0 + k(\gamma)^n$$

Where τ, τ_0, k, γ and n represents shear stress, yield stress, consistency constant, shear rate and power law index respectively.

2.3.1 Calculation of yield stress

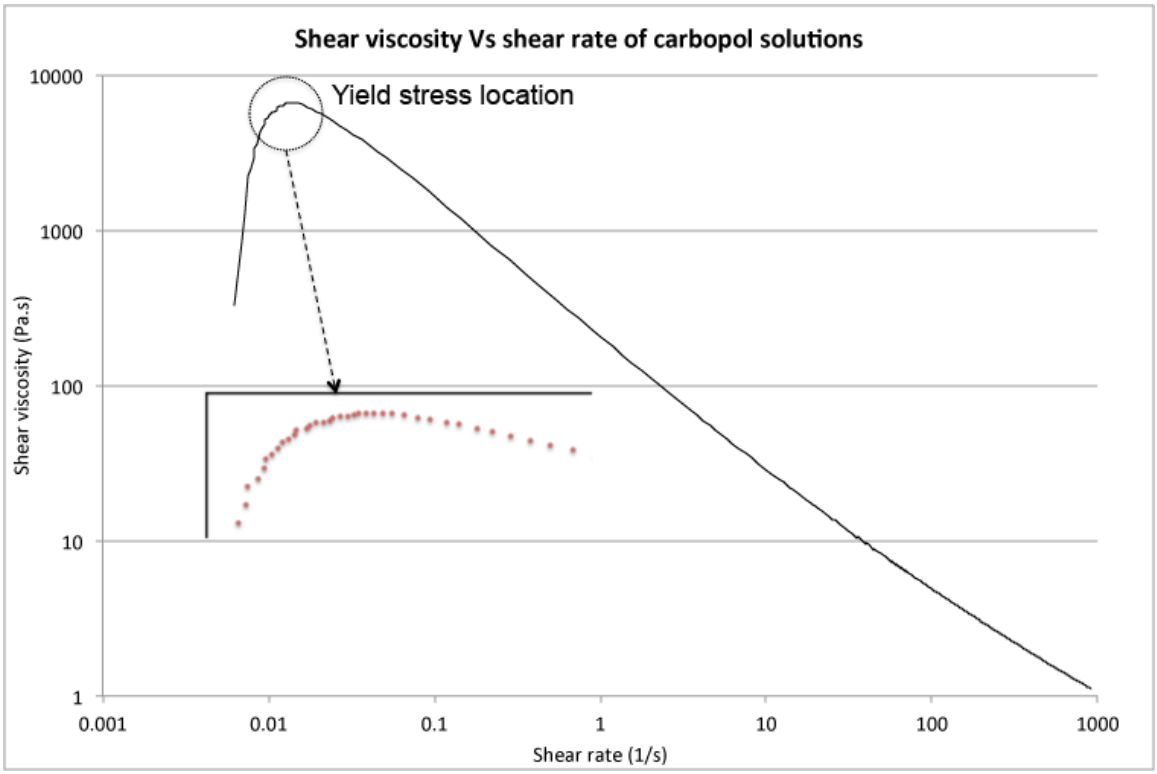

Figure 1 Prediction of the yield stress of the Carbopol solutions using a shear viscosity versus shear rate curve

Bohlin CS 30 rheometry software provides the shear stress and instantaneous viscosity values for every shear rate in the range. Because the literature shows that Carbopol gels follow the Hurschel – Bulkley viscosity model, we use the MATLAB® curve fitting toolbox to fit the obtained data into a Hurschel – Bulkley equation, thereby calculating the yield stress, consistency constant and power law index. The yield stress can also be calculated by plotting the shear viscosity versus shear stress curve on a log scale. At yield stress the viscosity will be at a maximum, after which the curve will show shear thinning behavior. The yield stress value and shear viscosity vs shear rate level are very close in value. Here we report values derived from our plots.

Seven Carbopol – water solution samples were prepared to achieve different yield stress, consistency constant and power-law index levels, and to study the effects of these variables on jet impingement on a moving surface. All of the liquids and their properties are listed in Table 1.

Table 1 Rheological properties of Carbopol solutions

Name	Percentage of Carbopol	pH of solution	Yield stress (Pa)	Consistency constant (k)	Power law index (n)
C-0.1	0.1	5.30	10.44	6.178	0.285
C-0.2	0.2	5.70	45.14	33.08	0.29
C-0.3	0.3	5.70	55.32	51.47	0.31
C-0.4	0.4	5.30	61.47	58.03	0.32
C-0.5	0.5	5.20	70.78	67.69	0.33
C-0.6	0.6	5.30	76.47	69.36	0.35
C-0.7	0.7	5.20	91.76	83.24	0.36

Table 1 shows that as the percentage of Carbopol in the solution increases the yield stress, consistency constant increase and power-law index increase. The rheological properties of the Carbopol solution also depend on the pH of the solution. From our experiments we found that the optimal gel-like Carbopol solution is achievable only if the pH of the solution is in range of 5.0 – 6.0. Below 4.0 and above 6.5, solutions show very small or almost negligible yield stress, while the power-law index becomes quite high (close to one). In other words, the solution behaves like a Newtonian solution.

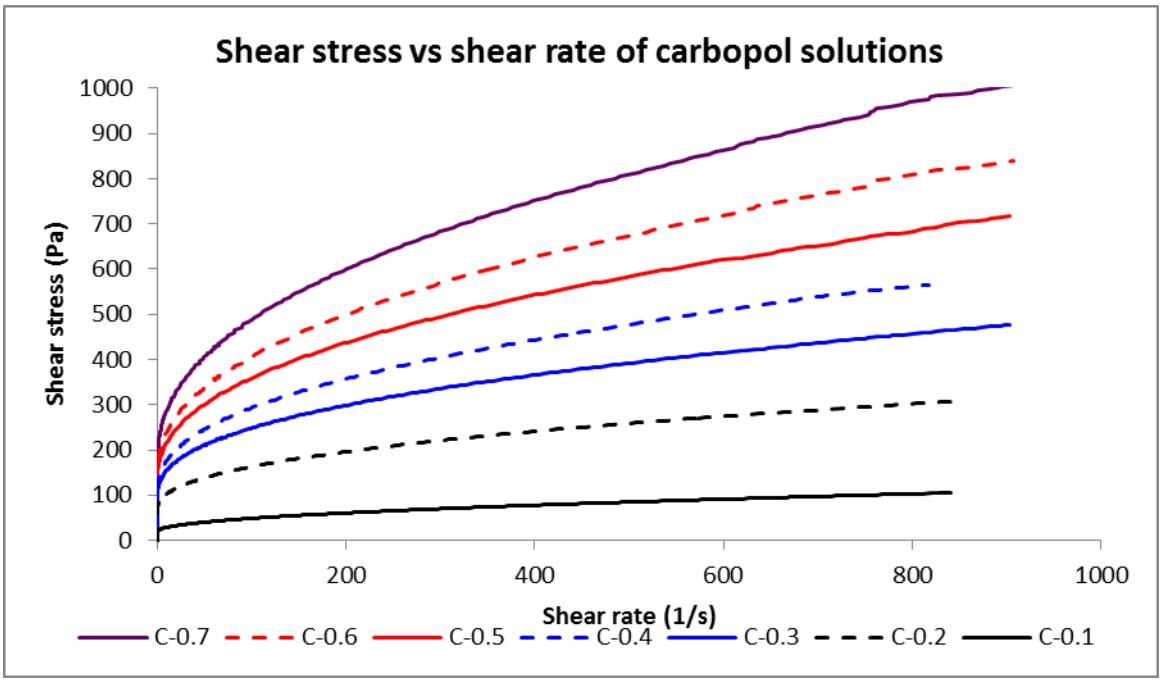

Figure 2 Shear stress versus shear rate curves for different Carbopol solutions

Figure 2 shows the shear rate versus the shear stress curves of the Carbopol liquids tested, arranged by increasing yield stress from bottom to top. The figure shows that the yield stress of each sample solution depends on the percentage of Carbopol in the liquid, as long as the pH of the solution is in the optimal range (5.0 – 6.0). It can be observed that the slope of the lines (power law index) changes with an increase in the percentage of Carbopol.

2.4 Apparatus and method

The liquid jet was generated with the help of a bladder accumulator, connected to a valve (to regulate the flow rate) and a nozzle with an internal diameter of 648 μm. A high-speed liquid jet was projected when the nozzle opened, and the jet eventually impacted on a fast moving projectile. The surface velocity was achieved with the help of a pressurized air tank and steel barrel. Air was filled into air tank until the pressure inside the tank reaches 15 psi. Then the projectile shown in figure 4 is pushed inside the steel barrel. The projectile has a rubber attached at its back to insure proper seal between steel barrel and projectile. Once the poppet valve is opened compressed air from air tank rushes to the steel barrel and projectile gets pushed forward giving us a surface speed. The surface speed is non-linearly related with air tank pressure.

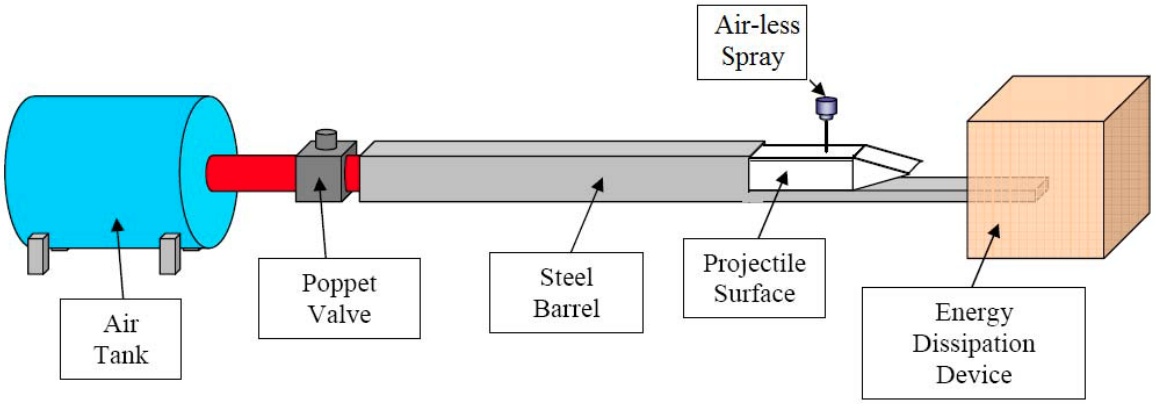

Figure 3 Layout of experimental setup

The projectile (Figure 4) was covered with a 13 mm thick polished steel surface (the top surface of an AREMA 136# rail) and fastened to a wooden base carrier. The jet issues at 25°C from a height of 15 mm and impinges on the moving surface perpendicularly.

Figure 4 Projectile with steel surface attached

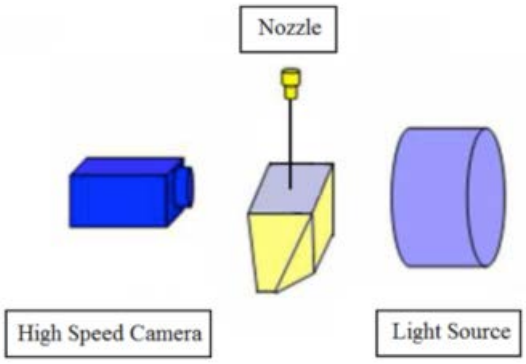

Figure 5 Light source and high speed camera assembly

We use a high power light source to illuminate the impingement surface and a high-speed camera to capture the activity at the surface. The high-speed camera enabled us to capture images at 6000 frames per second, at a 1280 by 854 resolution. Splash and deposition were clearly distinguishable using these settings. The projectile velocity was measured through image analysis of the high speed captured images. Jet diameter was also measured using high speed magnified images of the jet at various heights from the nozzle exit. The captured images were then analyzed through an image processing code written in MatLab®. The jet diameter was measured at different nozzle back pressures and for different fluids. The experimental setup used by Keshavarz [28] and Dressler [29] was also used here.

2.5 Results and discussion

2.5.1 Flow rate measurement

Flow rate measurement experimentation is an integral part of this research work. With our existing set up, this is the only way that we can obtain the jet velocity for the applied nozzle pressure. As explained previously, in our experimental setup, pressure is applied to the liquid and nozzle with the use of a compressed air cylinder and bladder accumulator. A controllable valve increases and a bleed valve releases the pressure inside the accumulator. These valves can control pressure in the range of ± 0.25 psi.

To measure mass flow rate, we used a stopwatch and weight balance. For each experiment we started the flow and took pressure measurements using a pressure transducer and data acquisition system. We then collected the liquid coming out of the nozzle into a container for 60 seconds. Using the weight balance and stopwatch we were able to calculate the mass flow per second. This experiment was repeated three times at each pressure to reduce error. Since the nozzle diameter and fluid density is known we were able to calculate the jet velocity.

$$Mass\ flow\ rate\ (\dot{m}) = \frac{mass\ in\ container\ (in\ 60\ seconds)}{60} \quad (2.1)$$

$$Jet\ velocity\ (V_j) = \frac{\dot{m}}{(\rho * \frac{\pi D^2}{4})} \quad (2.2)$$

Mass flow rate measurement also provides insight into the friction losses occurring within the nozzle. By calculating the mass flow rate versus the pressure we can locate any cavitation in the flow. The following chart measures the mass flow rate (grams per second) against pressure (psi), arranged by increasing the yield stress and consistency constant from top to bottom.

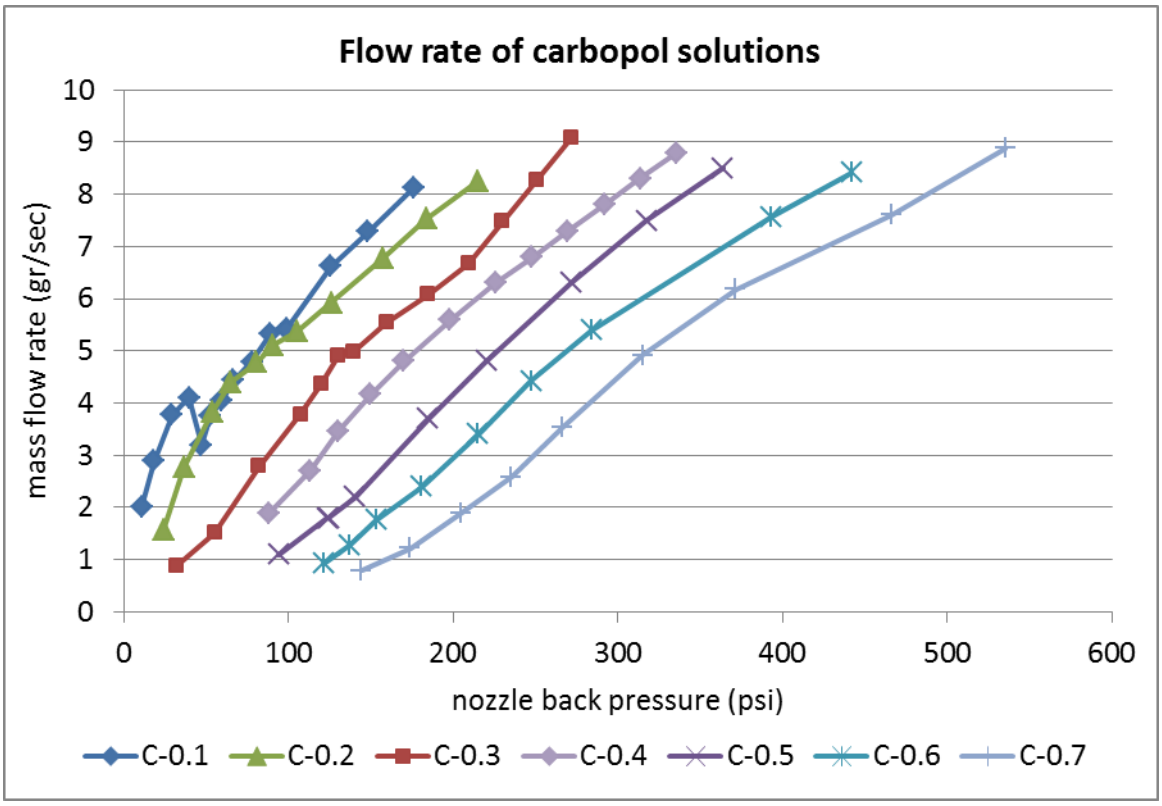

Figure 6 Mass flow rates of different cabopol solutions

Figure 6 shows the results of the mass flow rate versus pressure for different Carbopol solutions. Figure 6 and Table 1, demonstrate that as the yield stress and consistency constant (k) of the solution increase, the mass flow rate (at certain pressures) decreases.

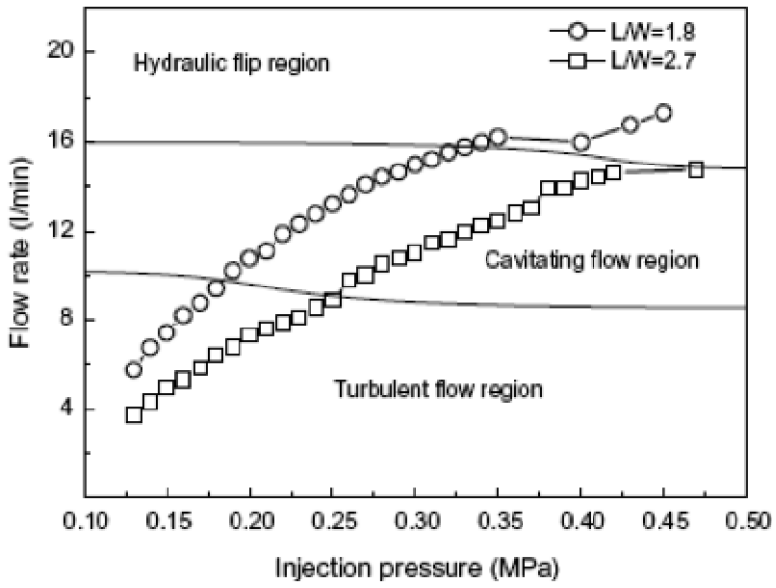

Figure 7 Mass flow rates in cavitation and hydraulic flip regions [30]

Figure 7 also shows that as the pressure for C-0.1 (solution with low yield stress and low viscosity) increases, the mass flow rate at first follows the Bernoulli principle by increasing, but later contradicts the principle by subsequently decreasing.

Other authors [30,31] that have observed this behavior have attributed this phenomenon to the cavitation of fluid inside the nozzle.

No other liquids showed any sign of cavitation, likely due to the higher value of consistency constants. Hence, viscosity, when kept at the same speed, is large enough to suppress the cavitation of the liquid.

2.5.1.1 Calculation of the discharge coefficient

Losses in fluid flow can be calculated by the discharge coefficient. Here we report the discharge coefficient with respect to the Reynolds number (Re). The Re has been calculated based on the average viscosity in the nozzle.

$$Discharge\ coefficient\ (C_d) = \frac{Experimental mass\ flow\ rate\ (\dot{m})}{Theoretical\ mass\ flow\ rate} \tag{2.3}$$

Experimental mass flow was obtained from the experiments explained above.

$$Theoretical\ mass\ flow\ rate = \rho * \frac{\pi D^2}{4} * \sqrt{\frac{2\Delta P}{\rho}} \tag{2.4}$$

$$C_d = \frac{\dot{m}}{\rho * \frac{\pi D^2}{4} * \sqrt{\frac{2\Delta P}{\rho}}} \tag{2.5}$$

$$Re = \frac{\rho V_j D}{k\left(\frac{V_j}{2D}\right)^{n-1}} \tag{2.6}$$

Figure 8 calculates the discharge coefficient and Reynolds number for each liquid based on the above expression. The discharge coefficients increase with an increase in the Reynolds number. This shows that as the viscosity decreases, the viscous losses in the nozzle also decrease. After observing the plot we noticed that the discharge coefficient begins to decrease after Re reaches 2000, and then increases again after Re reaches 3000. This behavior again occurs due to cavitation inside the nozzle. This behavior has also been observed for Newtonian liquids with lower viscosities [28].

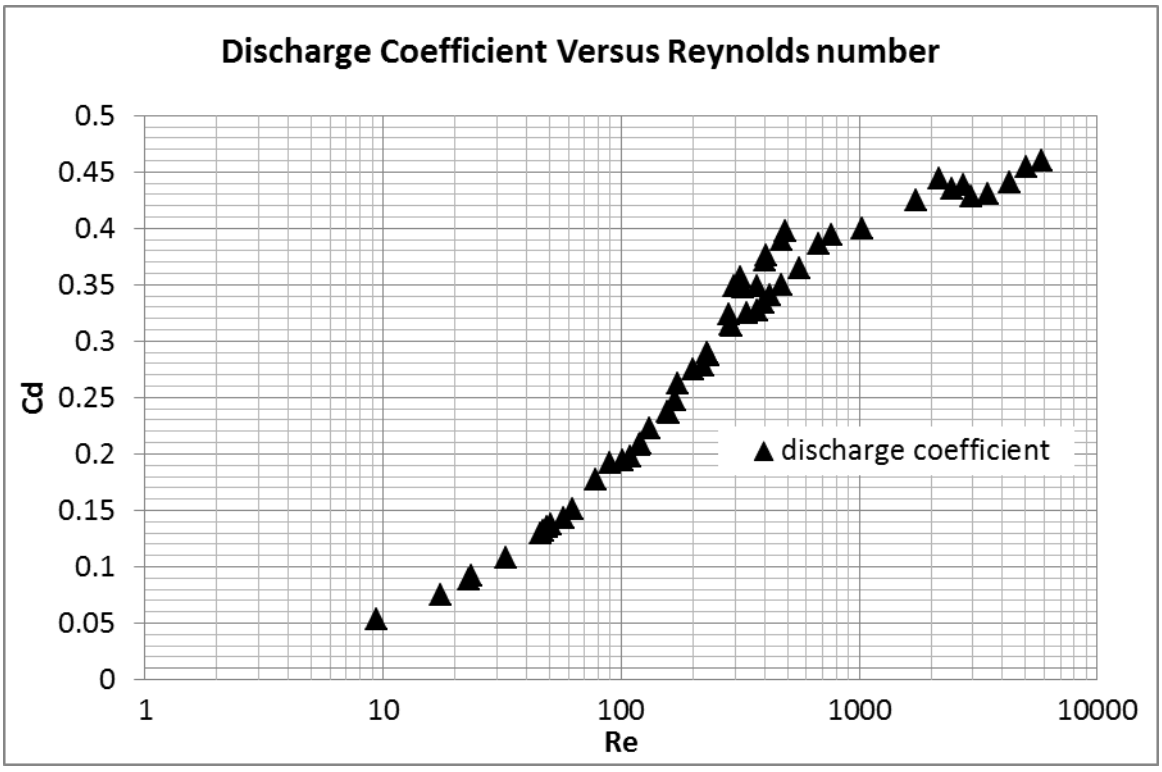

Figure 8 Discharge coefficient of Carbopol solutions with 648micron nozzle

2.5.2 Splash – deposition experiment

The interaction of a non-Newtonian liquid jet with a moving surface was captured using a high-speed camera. The Phantom® V12 camera with an image resolution of 1280 X 854 and 6300 frame per second speed was used to capture these images. A 100-watt LED light source with a light filter illuminated the impingement surface. The liquid jet diameter was approximately 650 micron, and the spread width in front of the jet was about 20-jet in diameter. The gap between the nozzle and the impingement surface was 10 centimeters. Given these distances, the field of view of the camera was kept at 20 cm (width) X 10 cm (height). Splash and deposition were easily distinguishable in images captured using these settings.

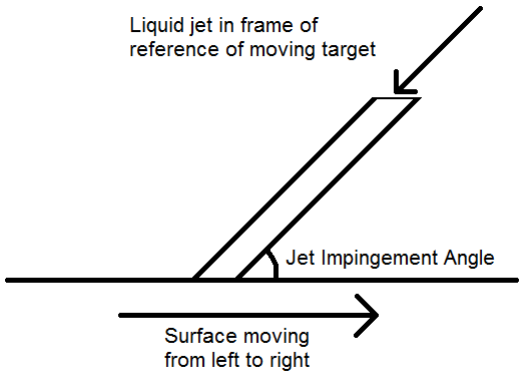

Figure 9 A Liquid jet impinging on a moving surface

Figure 9 shows the schematic of the jet impingement in the frame of reference of the surface. At a certain time the liquid jet will always appear to be impacting on to the surface at 90 degree but the velocity vectors will be certain angle with the resultant velocity and that angle is called jet impingement angle. The outcome of jet

impingement depends on jet velocity (V_J), surface velocity (V_S), liquid density (ρ), dynamic viscosity (μ), yield stress (τ), surface tension (σ) and surface roughness (ε) and jet diameter (D_{Jet}). These dimensional parameters make five dimensionless parameters. We have been able to study effects of four dimensionless parameters such as Reynolds number (Re), Weber number (We), Oldroyd number (Od) and Jet impingement angle (α) in this study. The effects of surface roughness ratio have been studied by Keshavarz [28] and increase in surface roughness ratio decreases the splash threshold considerably. Relative jet velocity and lamella thickness has been used as velocity and length scale for both Reynolds and Weber number. The lamella thickness here is assumed as tenth of jet diameter and that is why $0.1 \cdot D_{jet}$ is taken in the expressions mentioned below.

$$Re = \frac{\rho V_{rel}(0.1 \cdot D_{jet})}{k \cdot \left(\frac{V_{rel}}{0.1 \cdot D_{Jet}}\right)^{n-1}} \tag{2.7}$$

$$We = \frac{\rho \cdot V_{rel}^2 (0.1 \cdot D_{jet})}{\sigma} \tag{2.8}$$

$$Od = \frac{\tau}{k \cdot \left(\frac{V_{rel}}{0.1 \cdot D_{jet}}\right)^n} \tag{2.9}$$

$$Jet\ Impingement\ Angle = \left(\tan^{-1}\left(\frac{V_J}{V_S}\right)\right) \cdot \frac{180}{\pi} \tag{2.10}$$

Where V_{rel} is defined as $\sqrt{V_J^2 + V_S^2}$, the jet diameter is 648 microns.

For each individual liquid we started experiments at lower jet and surface velocities, increasing the speed by small increments in subsequent experiments. At smaller jet and surface velocities, jets deposit, and at relatively higher velocities jets begin to splash. To find the splash threshold for the individual liquids we investigated splash in the vicinity of (± 5 m/s velocity) and analyzed the images obtained. From our experiments we found that if splash has been observed at a certain speed (for example, at 15 m/s jet speed and 5 m/s surface speed) the impingement

outcome will always be splash if velocities have been increased for the same liquid. In other words, for individual liquids there is never more than one splash threshold.

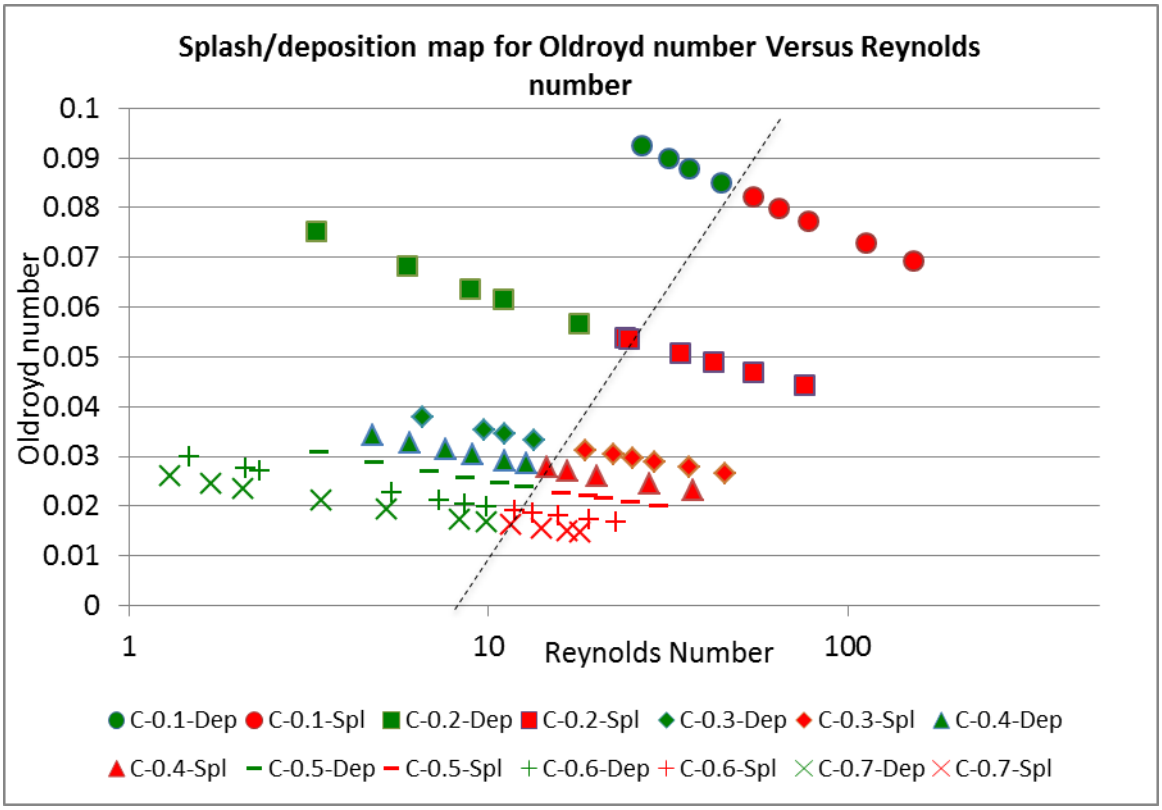

Figure 10 Effects of the Reynolds number and Oldroyd number on splash-deposition results of Carbopol solutions

Figure 10 represents the splash-deposition results for different Carbopol solutions emitted through a 648 micron nozzle. The Oldroyd number and Reynolds number are directly related to the yield stress and viscosity respectively. In Figure 10 each line represents an individual liquid, with the top and bottom lines representing the results of the C-0.1 (yield stress = 10.44, k = 6.178) and C-0.7 (yield stress = 91.76, k = 83.24) solutions respectively. On each line the leftmost and rightmost points represent lowest and highest relative velocity respectively.

Figure 10 clearly shows that there is a splash threshold for each liquid and that it varies with the yield stress and consistency constant of the liquid. An approximate boundary between the splash and deposition points is a straight line with a positive slope that shows that the splash threshold of the liquid is dependent on both the Reynolds number and the Oldroyd number. This also means that as the yield stress of the liquid increases, the minimum Reynolds number to

cause splash also increases. Therefore, an increase in the yield stress and consistency constant inhibits splash.

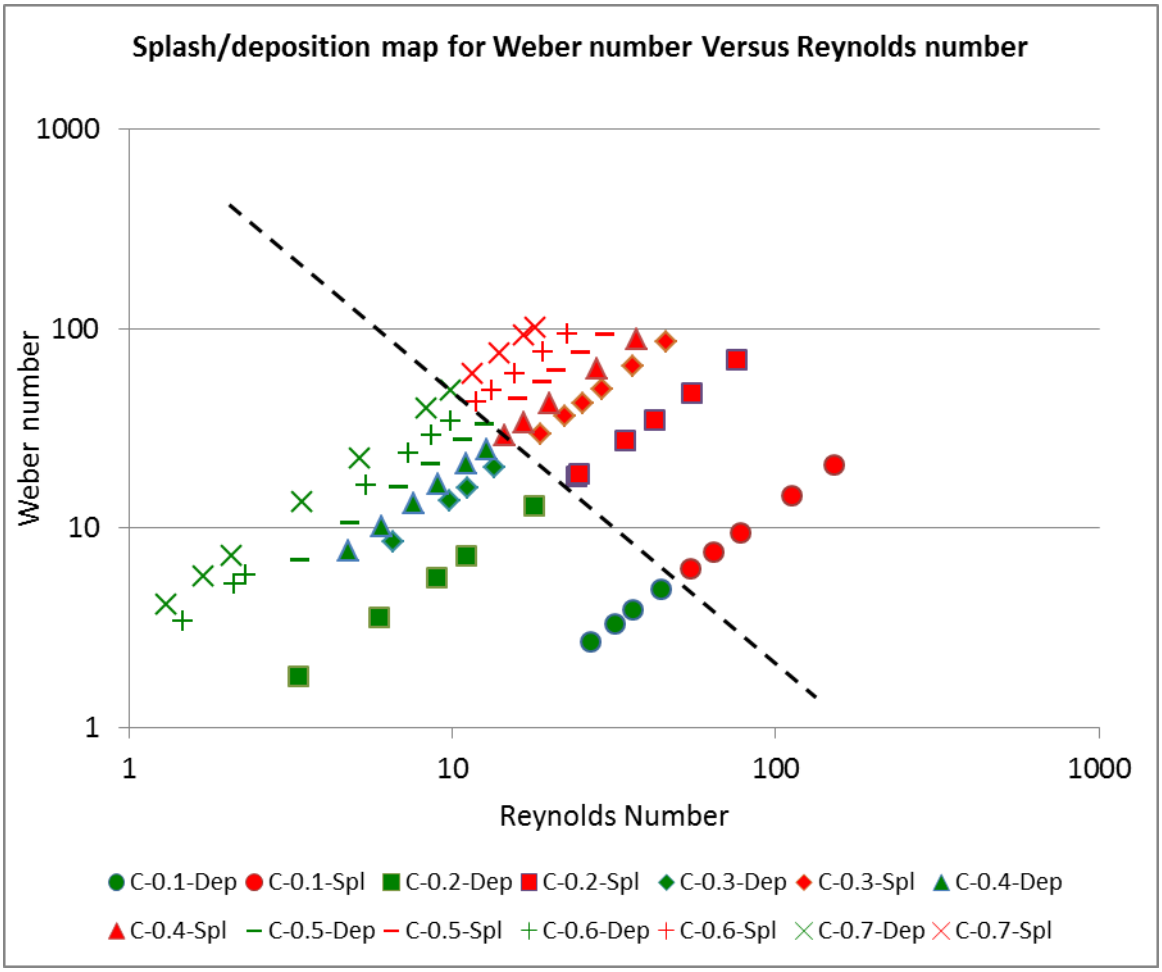

Figure 11 Effects of the Weber number and Reynolds number on splash-deposition results of Carbopol solutions

Figure 11 demonstrate the results of a splash-deposition experiment on a Weber number versus Reynolds number curve. An approximate boundary between splash and deposition points illustrate that it has a power law relation between Re and We number for splash threshold. It can also be inferred from nature of power law curve that at low Reynolds numbers the effect of the Weber number is almost negligible, and at high Reynolds numbers the effect of the Weber number becomes prominent. This is also reasonable because at low Reynolds numbers the viscous forces are higher than the surface tension forces. Thus, most of the inertial forces are balanced by the viscous forces. However, at high Reynolds numbers the lamella thickness (thickness of the liquid sheet generated on the moving surface by the impinging jet) becomes

very thin making larger surface area; hence, forces applied by the surface tension become dominant and the effect of the Weber number starts to appear. Therefore, the effect of the Weber number is dominant at low Weber numbers only.

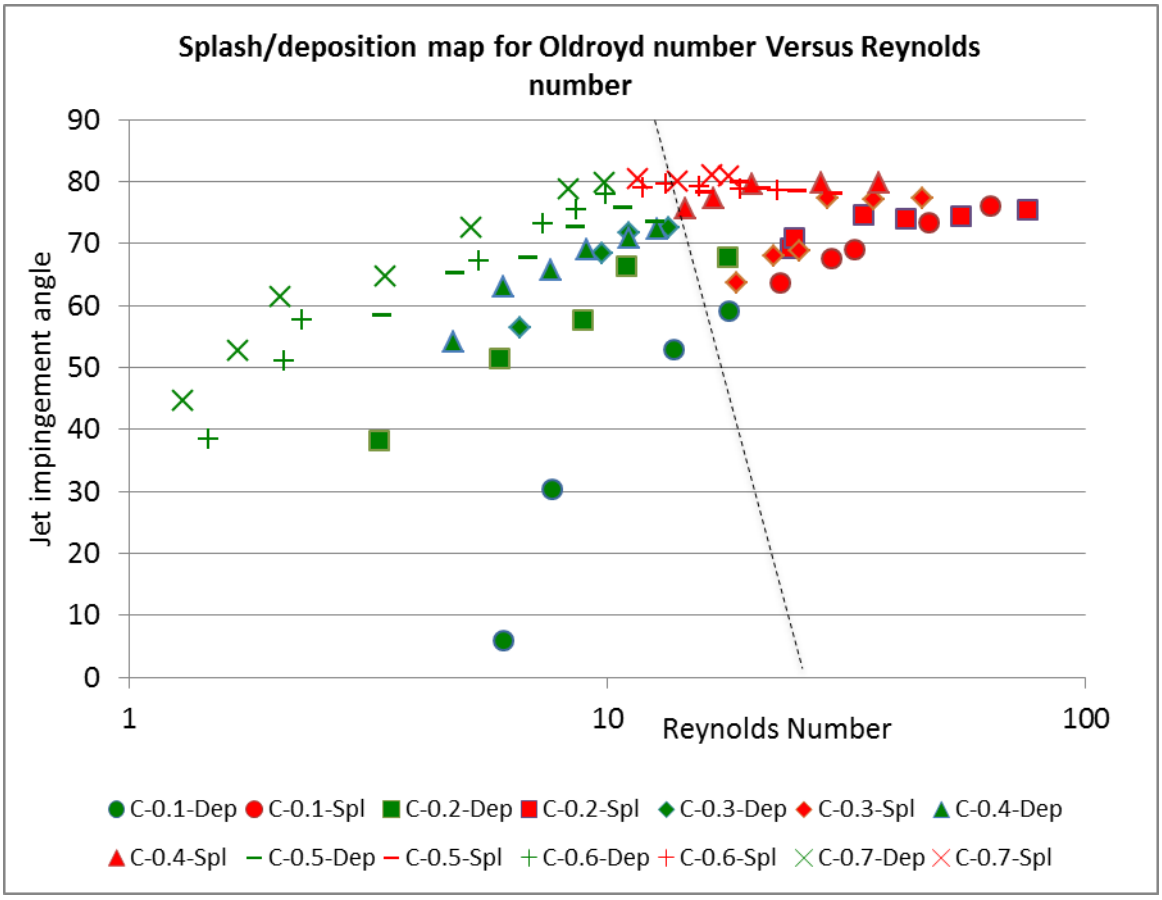

Figure 12 Effects of the jet impingement angle and Reynolds number on splash-deposition results of Carbopol solutions

It is clear from Figure 12 that an approximate boundary exits between splash and deposition points here as well. The approximate boundary is a straight line with a negative slope close to 90°. Referring to this approximate boundary it can be inferred that the effect of the jet impingement angle is much less significant compared to effect of the Reynolds number. Our experiments also show that the jet impingement angle has an almost negligible effect compared to the effect of the Reynolds and Oldroyd numbers. The effect of jet impingement is perceivable only at very low surface speeds. Otherwise, only the combined jet and surface speed is responsible for splash/deposition behaviour.

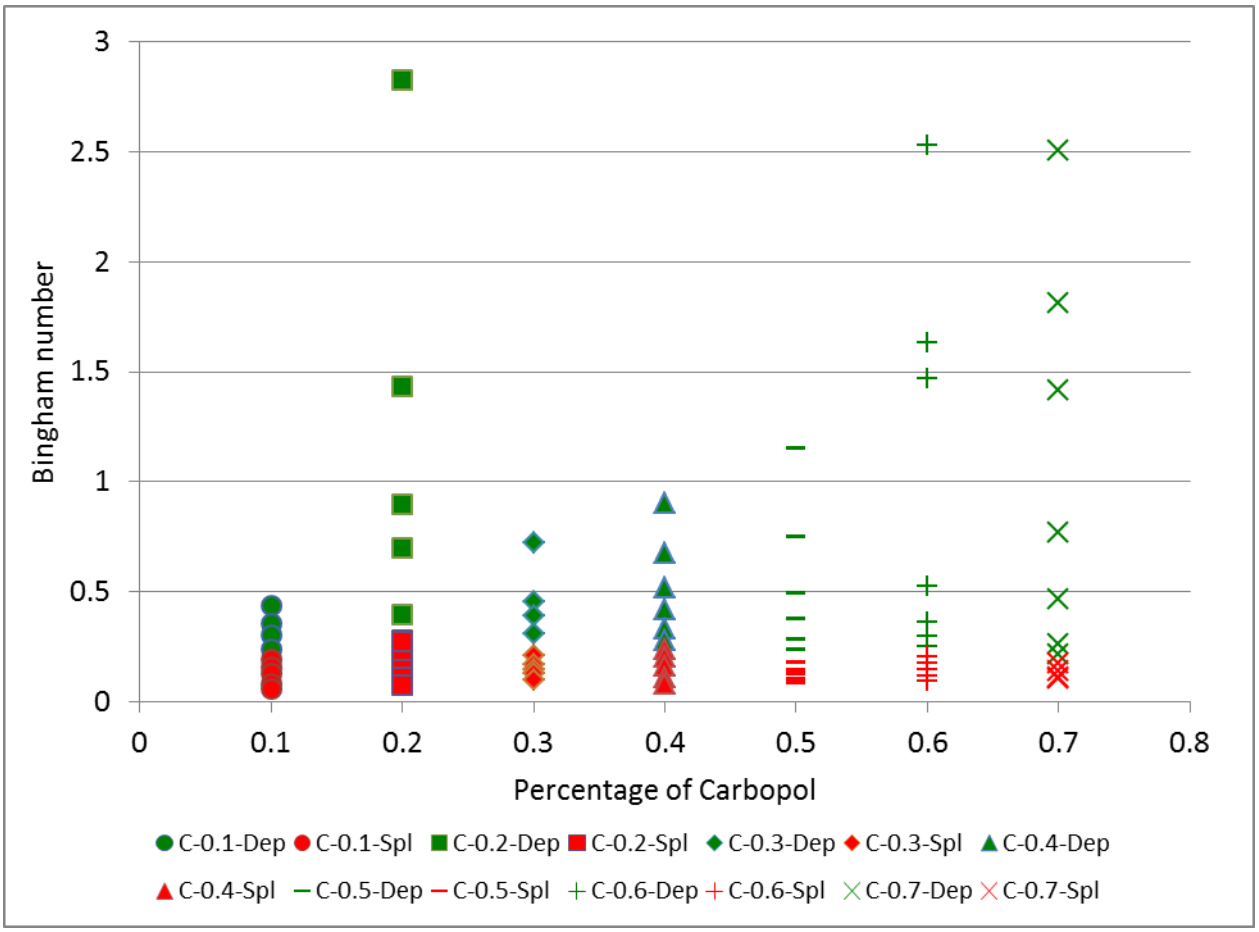

Figure 13 Effect of Bingham number on splash threshold

Above figure shows that when Bingham number ($\tau_0/0.5*\rho V^2$) is greater than 0.3 the liquid jet results in deposition but when it is below that number it starts to splash. It also illustrate that increase in percentage of the Carbopol has very little effect on the splash threshold; but the splash threshold is almost constant.

2.6 Summary

The impaction of a free-surface jet of non-Newtonian fluid onto a moving surface has been investigated experimentally. A high-speed jet was generated through a 648 micron nozzle and the splash dynamics on the moving surface were captured using a Phantom® V12.1, high-speed camera. In particular, the study focuses on the effects of the jet velocity, surface velocity, and fluid properties on the splash/deposition characteristics of the jet. Several different Carbopol solutions with varying yield stress, consistency constant and power-law indices were tested. The yield stress, consistency constant, power-law index, jet velocity and surface velocity for these experiments ranged from 10-90 Pa, 6-85, 0.28-0.36, 5-40 m/s and 5-15 m/s respectively. The

combination jet velocity, surface velocity and fluid properties gave a wide range of Re (1 – 100), Od (0.01-0.1) and We (1 – 120).

The key findings of these experimental studies are:

- Both jet speed (normal speed) and surface speed (tangential speed) play roles in the splash or deposition of the jet on a surface.
- Both the yield stress and consistency constant of the liquids are important in balancing the inertial force of the jet.
- The effects of the jet impingement angle are negligible compared to the effects of the jet relative velocity and fluid properties.
- The surface tension forces are dominant compared to the viscous forces only at low Weber numbers.
- An increase in yield stress and consistency constant inhibits lamella splash.

Chapter 3 - Newtonian Liquid Jet Interactions with a Moving surface

3.1 Introduction

The behavior of a Newtonian liquid jet impinging on a moving surface has been studied experimentally by means of high-speed imaging. In particular, this study focuses on the role of the shear viscosities and surface tensions of Newtonian liquids, the resultant velocity of the jet and surface, jet diameter, and jet impingement angle, on the splash-deposition characteristics of a liquid jet impingement. Several Newtonian liquids including water-glycerin and water-propylene glycol solutions with wide ranges of shear viscosities and surface tensions were used to understand the effects of underlying parameters. Two nozzles with 200 and 400 micron diameters were used to understand effect of jet diameters. The jet and surface speed of this experimental study ranges from 5 – 40 and 5 -15 m/s respectively. With these experimental settings we were able to analyze effects of several dimensionless parameters (Reynolds number, Capillary number, and Jet impingement angle).

The experimental results show both jet and surface speeds play roles in behavior of jet impingement. We also observed that low (water) and high (glycerin) viscosities liquid jet deposits on the target surface even at 40 m/s but mid-range viscosity (water-35%+glycerin-65% to water-60%+glycerin-40%) liquid jets starts to splash at 15 m/s. From high-speed video we understood that the thickness of the liquid spread on the target surface is function of viscosity and it increases with increase in viscosity. It was also observed that effects of surface tension become dominant for lower viscosities liquids and effects of viscosity becomes dominant for higher viscosities liquids. A mathematical explanation based on force balance on lamella is also obtained to show qualitative effects of viscosities on outcome of a jet impingement. Finally we also observed that the ratio of the velocities (Jet impingement angle) was not an important variable compared to resultant jet velocity. With this research work we are able to show that the decreasing the nozzle diameter decreases the application rate while keeping reasonable jet speed and it also provides better chances of deposition.

3.2 Experimental setup and test liquids prepared

The experimental setup explained and used in chapter 2 was also used to conduct research works reported here. The only difference in experimental setup is that we used smaller diameter nozzle (200 and 400 micron nozzle) instead of 648 micron nozzle.

Nine water-glycerin and five water-propylene glycol mixtures were prepared for these tests. Both the water-glycerin and water-propylene glycol solutions were mixed using double impeller rotational mixer for 24 hours. The Rheometry and surface tension measurements were taken 4 to 5 hours prior to the splash-deposition experiments. Because the water-glycerin mixtures do not degrade rapidly, a 4 to 5 hour gap between the Rheometry and splash-deposition experiments did not affect the results. We nonetheless measured viscosity at 2-hour intervals to account for any errors that may have occurred due to the time gap between experiments.

The fluid surface tensions were also measured by a Du Noűy ring apparatus at a temperature of 25°C; the surface tension values for all of the water-glycerin mixtures were close to that of water (72.1 mN/m), within a range of ± 5%. The surface tensions of the Water-propylene glycol mixtures were smaller than those of the water-glycerin mixtures. Liquid shear viscosities were measured using a Bohlin CS 10 Rheometer with a cone-plate arrangement, with a range of 1mPa.s to 88mPa.s. Since the shear viscosity ranged over two orders of magnitude, the Reynolds number of our experiment varied from 10 – 8000.

All of the Rheological properties of the water-glycerin and water-propylene glycol mixtures have been enlisted in Tables 2 and 3.

Table 2 Rheological properties of water-glycerin mixtures

Name	Percentage of glycerin in water	Density (kg/m^3)	Viscosity $(mPa \cdot sec)$	Surface tension (mN/m)
Water	0	1000	1	72.1
WG-20	20	1052.2	1.5	70.5
WG-30	30	1078.3	5.5	69.7
WG-40	40	1104.4	7.2	68.9
WG-50	50	1130.5	9.6	68.1
WG-60	60	1156.6	15.3	67.3
WG-65	65	1169.6	19.2	66.9
WG-70	70	1182.7	30.53	66.5
WG-85	85	1221.8	88.02	65.3

Table 3 Rheological properties of water-propylene glycol mixtures

Name	Percentage of propylene glycol	Density (kg/m^3)	Viscosity $(mPa \cdot sec)$	Surface tension (mN/m)
WPG-05	5	1001.8	1	56.7
WPG-40	40	1014.4	6.46	42.0
WPG-50	50	1018	9.20	41.1
WPG-60	60	1021.6	12.0	39.8
WPG-75	75	1027	20.7	38.8

3.3 Results and discussion

3.3.1 Flow rate measurement

In our experiments, we calculated the jet velocity using mass flow rate measurements. We estimated the mass flow rate using a precise balance and a stopwatch. The liquids at individual pressures were discharged for 60 seconds into a container of known weight. The weight of the liquid discharged was measured using a balance. Dividing the weight of the discharged liquid by 60, we calculated the mass flow rate of the liquid. This experiment was conducted for each liquid under pressures ranging from 10 – 150psi.

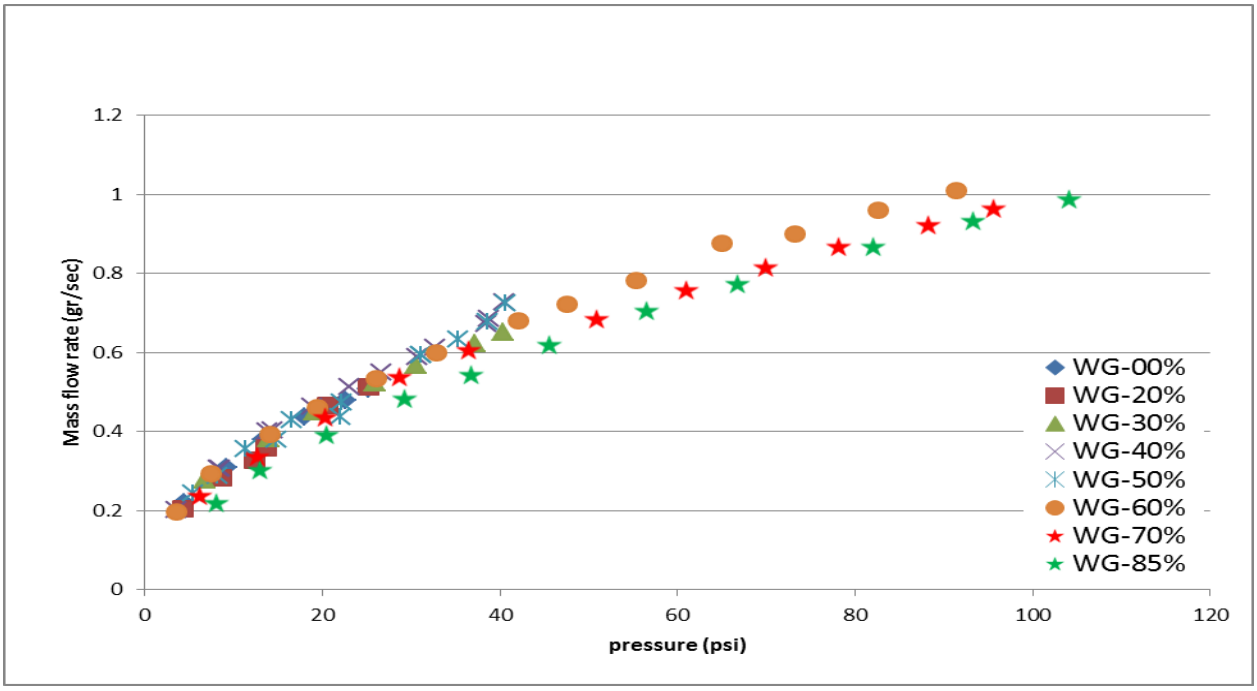

Figure 14 Mass flow rates of water-glycerin solutions through a 200 micron nozzle

As these experiments demonstrate, losses due to viscosity in the liquids dispensed through this nozzle were minor, and thus the mass flow rates of the different water-glycerin solutions were quite close in range. The experimental results are presented in Figure 14.

The mass flow rates of WG-00 - WG-50 solutions are similar because these liquids are close in viscosity levels. Between higher viscosity liquids from WG-60 - WG-85, mass flow rates begin to diverge. This behavior was predicted because the viscosity of these liquids changes from 15 mPa.s to 88 mPa.s as the percentage of glycerin increases from 60 to 85 percent. Mass flow rates vary only slightly at lower driving pressures.

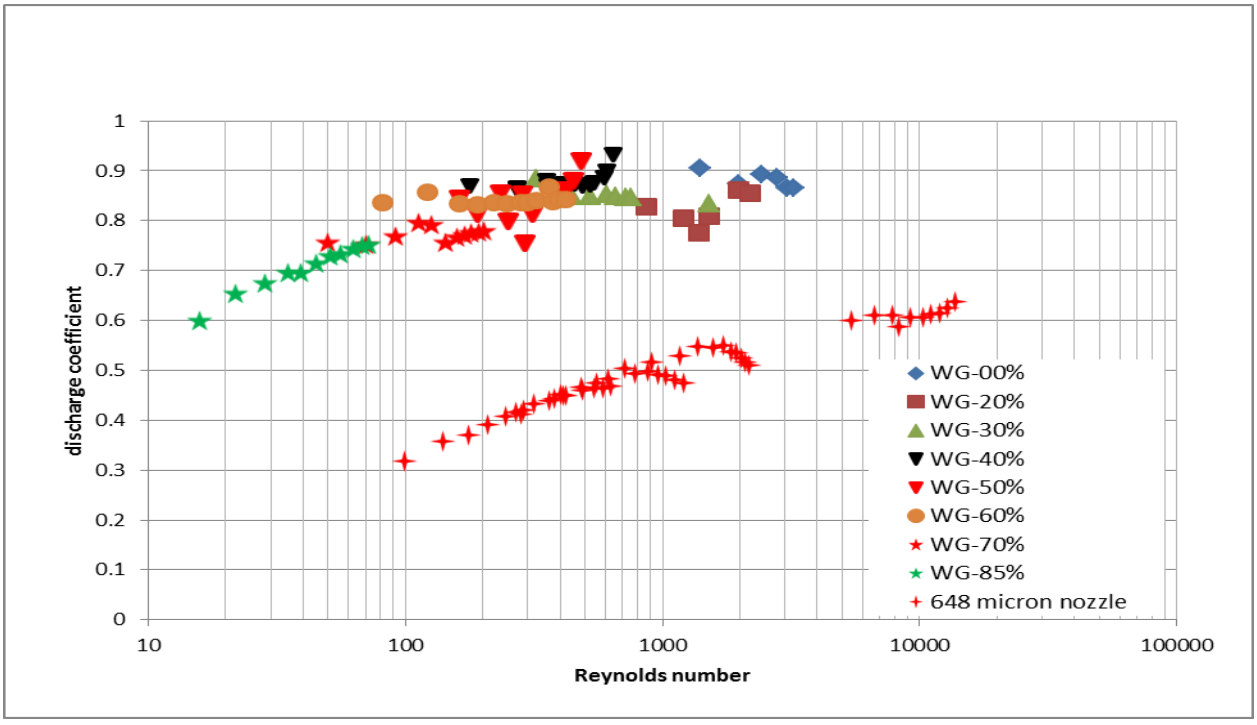

Figure 15 Discharge coefficient of water-glycerin solutions dispensed through 200 and 648 micron nozzles

In the above figure we have plotted the discharge coefficient, the measure of losses in the nozzle, with respect to the Reynolds number. We report both 200 micron and 648 micron nozzle data as a point of comparison. After observing the 200 micron nozzle data we find that as the Reynolds number of the flow increases the discharge coefficient also increases. This is related to the fact that viscous losses are more dominant at low Re levels than at high Re levels. When Re levels are 500 and higher there is first a decrease in the discharge coefficient, followed by an increase in its value. This behavior is attributed to the onset of cavitation, behaviour also reported by several previous authors [18-20]. For purposes of comparison we also show the

mass flow rates obtained using a 648 micron nozzle. The results show that the losses through the 648 micron nozzle are higher compared to those from the 200 micron nozzle. While it is known in fluid mechanics that in the case of pipe flow, losses decrease as the pipe diameter increases, the deviations in these experimental results can be understood in reference to nozzle geometry.

A nozzle cap of standard geometry (Figure 16) was designed and manufactured to enable us to conduct experiments with different nozzle sizes (either a 200 or 400 micron nozzle) while using the same nozzle cap. Precision pinholes of different sizes were provided by Edmund Optics®. The geometry of the nozzle cap and precision holes are illustrated in Figures 16 and 17.

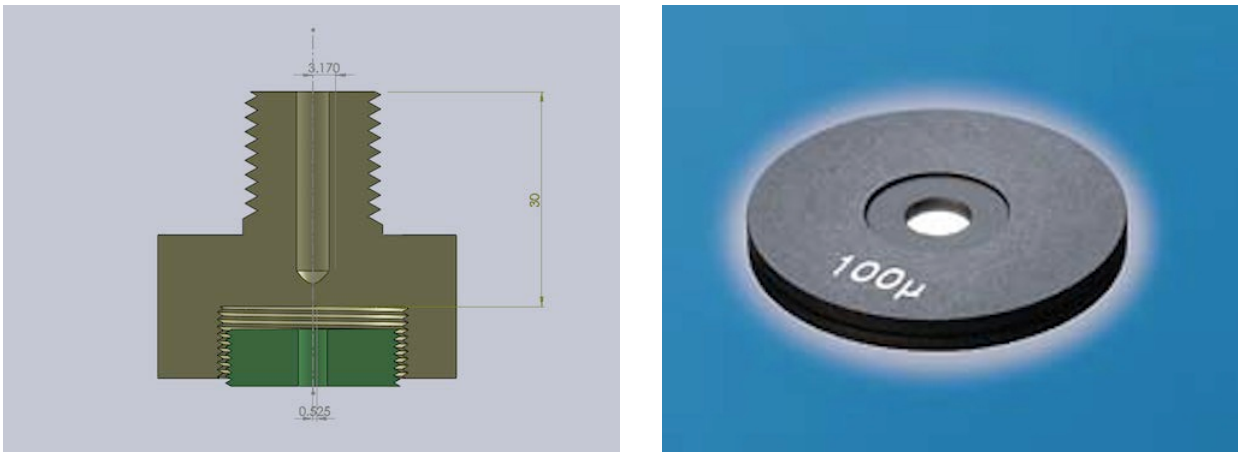

Figure 16 Nozzle assembly and precision pinhole

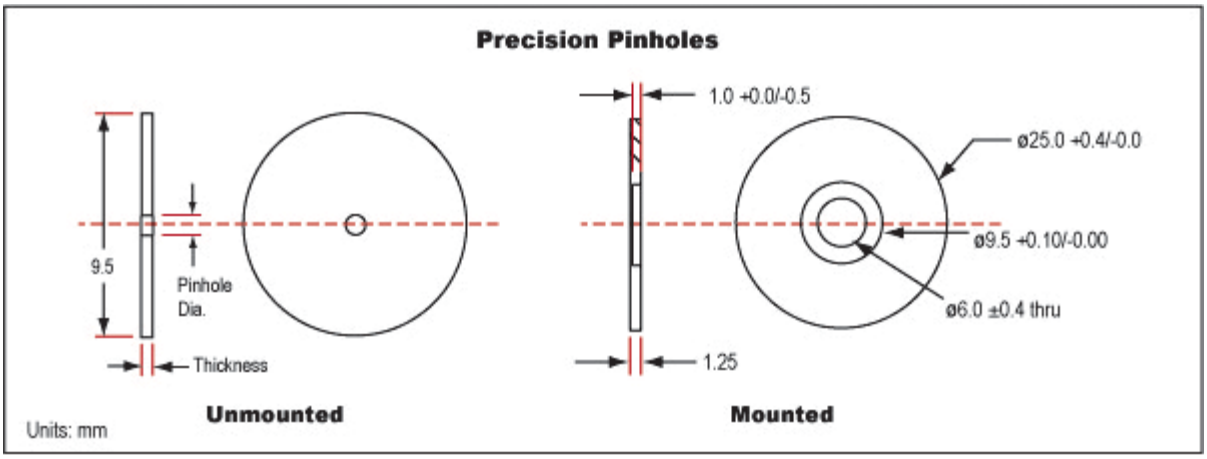

Figure 17 Geometry and dimension of the precision pinholes

The diameters of the precision holes are 200 and 400 micron, with thicknesses of 25 and 100 micron respectively. The 648 micron nozzle is 2 mm thick. Since the majority of the losses occur in smaller diameter section of the nozzles, the thickness or depth of the nozzle neck are critical

to our study. For the non-dimensional number, losses in the nozzle depend on the ratio of the nozzle thickness (H) to the nozzle diameter (D) i.e. H/D. The dimensions for three different nozzles are given in Table 4.

Table 4 Dimensions of three different nozzles

Nozzles	Diameter (micron)	Thickness (micron)	H/D	Type
200 micron	200	25	0.125	Sudden contraction
400 micron	400	100	0.25	Sudden contraction
648 micron	648	2000	3.08	Converging

The H/D values for the 200 micron and 648 micron nozzles are 0.125 and 3.08 respectively. It can therefore be concluded that losses, which are related to H/D, are larger for the 648 micron nozzle.

3.3.2 Spread radius, spread width and lamella thickness

Spread radius is defined as the maximum distance of a liquid surface in front of an impinging jet. Spread width is defined as the width of the liquid on either sides of a jet impinging on a moving surface. Both spread radius and width are shown in Figure 18.

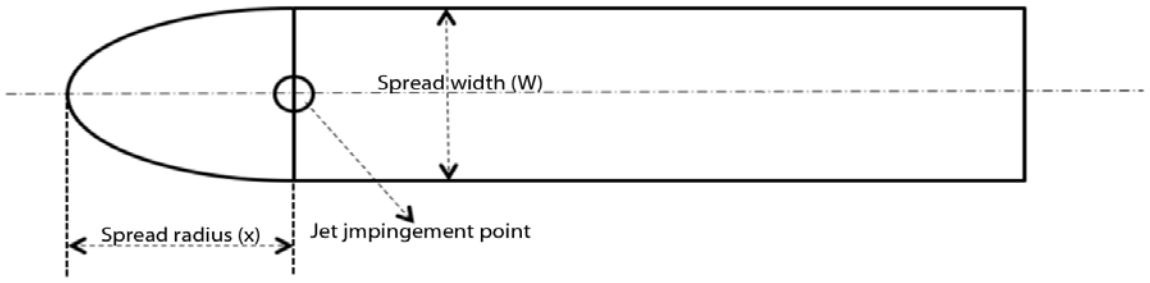

Figure 18 Simple representation of a liquid spreading on a moving surface

The spread radius in front of the jet (X) is elliptical, and the spread width on the either side of jet (W) is rectangular in shape with a wavy edge. The shape and dimensions of the spread depend on the fluid and flow properties. It has been observed that both the spread radius and width decrease with an increase in surface speed and fluid viscosity, and that the spread radius and width increase with an increase in jet speed and jet diameter.

Table 5 Spread radius and spread width of water for different jet and surface speeds

Row	Jet velocity (m/s)	Surface velocity (m/s)	Spread radius (X) in micron	X/D	Spread width (W) in micron	W/D
1	8.26	5.12	770	3.84	2440	12.2
2	10.8	5.29	1140	5.70	4033	20.1
3	11.3	9.84	1087	5.43	2865	14.3
4	18.7	5.19	1698	8.49	5519	27.6
5	18.7	10.1	1247	6.23	5201	26.0
6	24.6	5.31	1698	8.49	6262	31.3
7	25.6	9.98	1592	7.96	5838	29.1

Table 5 reports data recorded on a water jet generated through a 200 micron nozzle. In Rows 2, 3, 5 and 7, where surface velocities are close but jet velocities are increasing, the jet velocity rises, and the spread width both in front of and on the sides of the jet also increase. Rows 3, 4, 5 and 6 also illustrate that spread widths decrease with an increase in surface velocity.

Experiments were also conducted with other liquids such as WG-20, WG-30 and WG-85, using both 200 and 400 micron nozzles. It was found that increasing liquid viscosity decreases both spread radius and spread width.

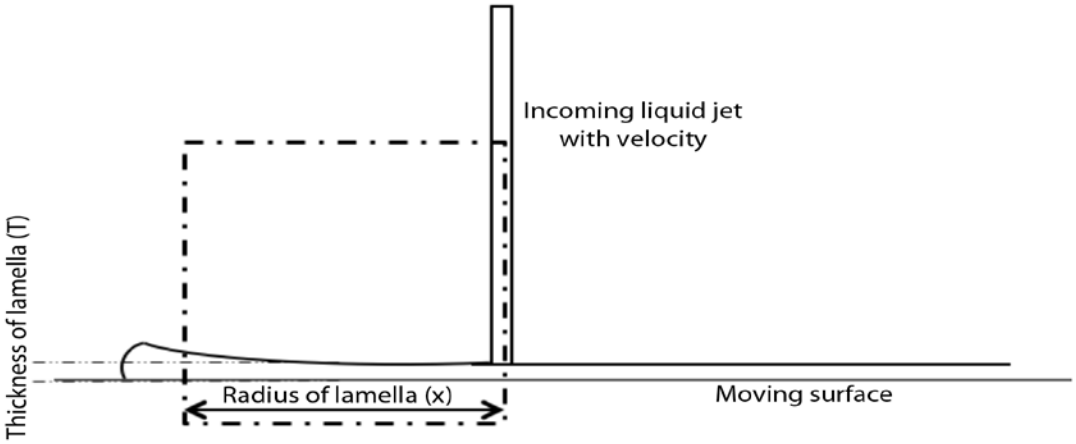

Figure 19 Representation of a jet spreading on a moving surface

Lamella thickness can be calculated roughly by applying a continuity equation between the incoming jet and the rate, at which the liquid spreads on the surface.

Assuming that half of the liquid spreads to the front and half of the liquid spreads to back of the jet. Therefore, the lamella thickness can be calculated using a mass balance formulation,

$$\frac{Mass\,flow\,rate}{2} = \pi r \cdot (thickness\ of\ the\ lamella) \cdot (velocity\ of\ the\ lamella) \quad (3.1)$$

The velocity of the fluid at any distance r from impingement point varies along its thickness due to boundary layer effect. However, due to the unavailability of information regarding the velocity profile of a lamella at any cross-section, we will apply this velocity as a constant and identify it as the average velocity at that radial distance. The lamella velocity will also vary along the radius. The velocity of the liquid in the vicinity of the impingement point will be very close to the jet velocity. The jet velocity will be equal to the surface speed at a far distance from the impingement point. Therefore, the velocity of the lamella will vary from the jet velocity to the surface velocity. Here, velocity variation is taken linearly,

$$V(r) = V_{jet} - \frac{V_{jet} - V_{surf}}{X - D/2} \cdot (r - D/2) \quad (3.2)$$

Where,

$V(r)$ is the velocity of the lamella at any distance r from the impingement point.

V_{jet} , V_{surf} and X represent the jet velocity, surface velocity and spread width in front of the jet.

Now lamella thickness at any distance r can be calculated using the equation given below,

$$T(r) = \frac{\dot{m}}{2\pi r} \cdot \frac{1}{V(r)} \tag{3.3}$$

Using expressions for $\dot{m}$ and $V(r)$ we will have,

$$T(r) = \frac{D_{jet}^2 \cdot V_{jet}}{8 \cdot r} \cdot \frac{1}{V_{jet} - \frac{V_{jet} - V_{surf}}{X - D/2} \cdot (r - D/2)} \tag{3.4}$$

Lamella thickness at r = X, i.e. where a liquid changes its direction of motion,

$$T(X) = \frac{D_{jet}^2 \cdot V_{jet}}{8 \cdot r} \cdot \frac{1}{V_{surf}} \tag{3.5}$$

3.3.3 Splash – deposition experiments

Using 200 and 400 micron nozzles, and water-glycerin and water-propylene glycol solutions, a series of experiments were conducted to study the interaction of a Newtonian liquid jet with a high speed moving surface. The jet velocity ranged from 5 – 40 m/s and the surface velocity ranged from 5 – 15 m/s. The Reynolds and Weber numbers, based on jet diameter, ranged from 10 – 8000 and 200 – 4000 respectively. The results showed that for water, and some low viscosity water-glycerin solutions, no splash occurred even at jet velocities as high as 40 m/s, or at surface velocities as high as 15 m/s. No splash occurred for high viscosity water-glycerin solutions, but for mid-ranged viscosity solutions splash occurred at relatively low velocities.

Figure 20 Impingement of water (left), WG-60 and WG-85 (right) jets (generated from a 200 micron nozzle) with jet speed of 15 m/s on a surface moving from left to right at 5 m/s.

It can be observed from Figure 20 that the water (left) and WG-85 (right) jets deposit on the surface, but the WG-60 jet splashes upon impaction. All of the experimental parameters, including surface temperature, jet speed and surface speed, were kept constant. It is also clear from the above figure that for low viscosity liquids, such as water, the length of the liquid surface

in front of the jet (or spread radius) is smaller than the spread radii produced by high viscosity liquids; e.g. WG-85.

It was observed that pure water to WG-30, and pure liquid glycerin to WG-75 jets deposited on the surface through a 200 micron nozzle very smoothly, and those liquids in the range of WG-40 - WG-65 began to splash at very low jet speeds.

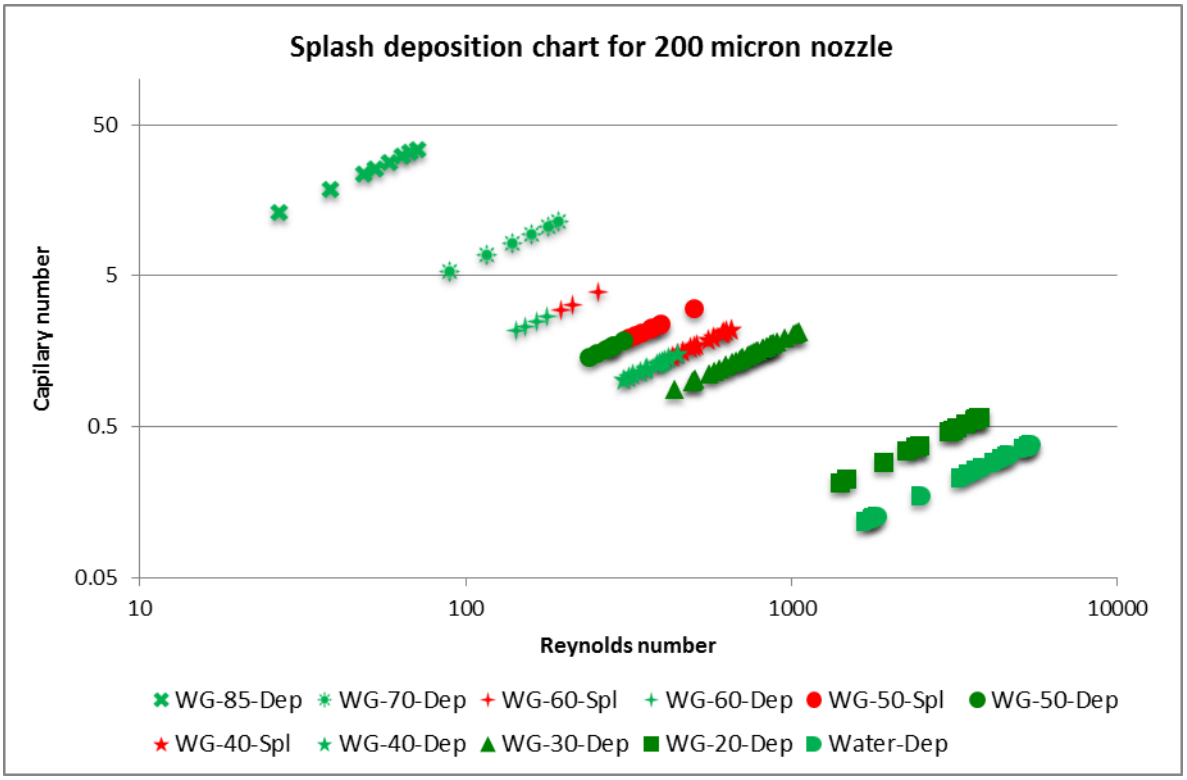

Figure 21 Effects of Re and Ca on the splash-deposition results of water-glycerin solutions dispensed through a 200 micron nozzle

Figure 21 clearly shows that splash-deposition results are dependent on both the Capillary number and Reynolds number. Liquid deposits when a low Re accompanies a high Ca, and when a high Re accompanies a low Ca. When a medium Re accompanies a medium Ca, however, both splash and deposition occur. For liquids such as WG-40, WG-50 and WG-60, the jet deposits on the surface at low Re and Ca levels, and starts to splash as the Re and Ca increase. For these three liquids, it was experimentally found that jets start to splash at a relative jet velocity of 13 m/s. For these liquids, the effect of the jet impingement angle also becomes significant i.e. at lower surface velocities (2-4m/s) jets start to splash at a relative velocity of 18 m/s, but at high surface velocities (5-7) jets begin to splash at a relative velocity of 10 m/s.

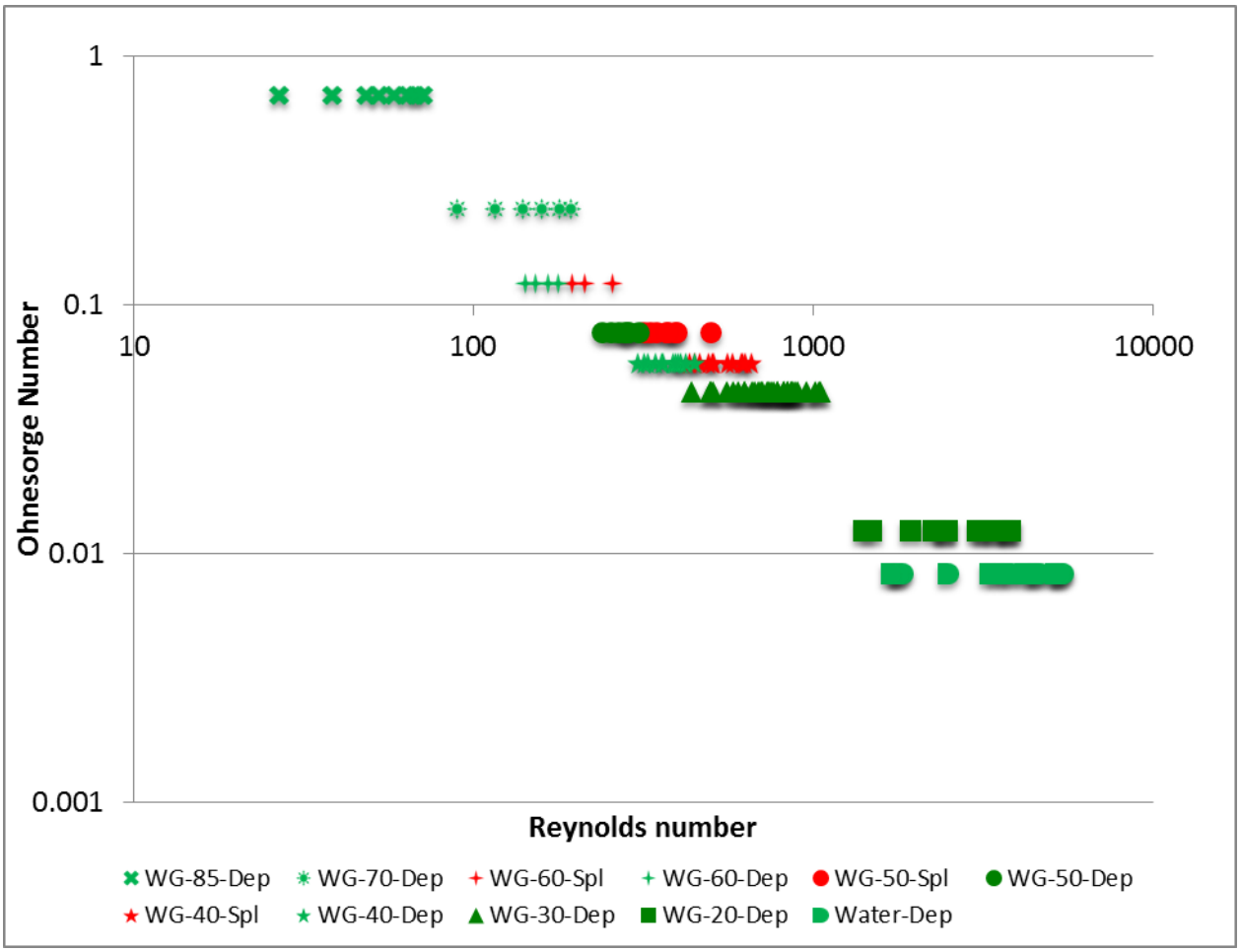

Figure 22 Effects of Reynolds and Ohnesorge number on the splash-deposition results of water-glycerin solutions dispensed through a 200 micron nozzle

Figure 22 shows the splash deposition results on Reynolds number versus Ohnesorge number plot. The Ohnesorge number ($Oh = \mu/\sqrt{\rho\sigma D}$) does not include velocity in its definition giving observation in forms of effects of velocity and nozzle diameter separately. Above figure clearly shows that as at low Oh and High Re, and high Oh and low Re results in deposition but intermediate Oh and Re gives both splash and deposition. It can also be understood from above figure that both Oh and Re play role in splash deposition characteristics.

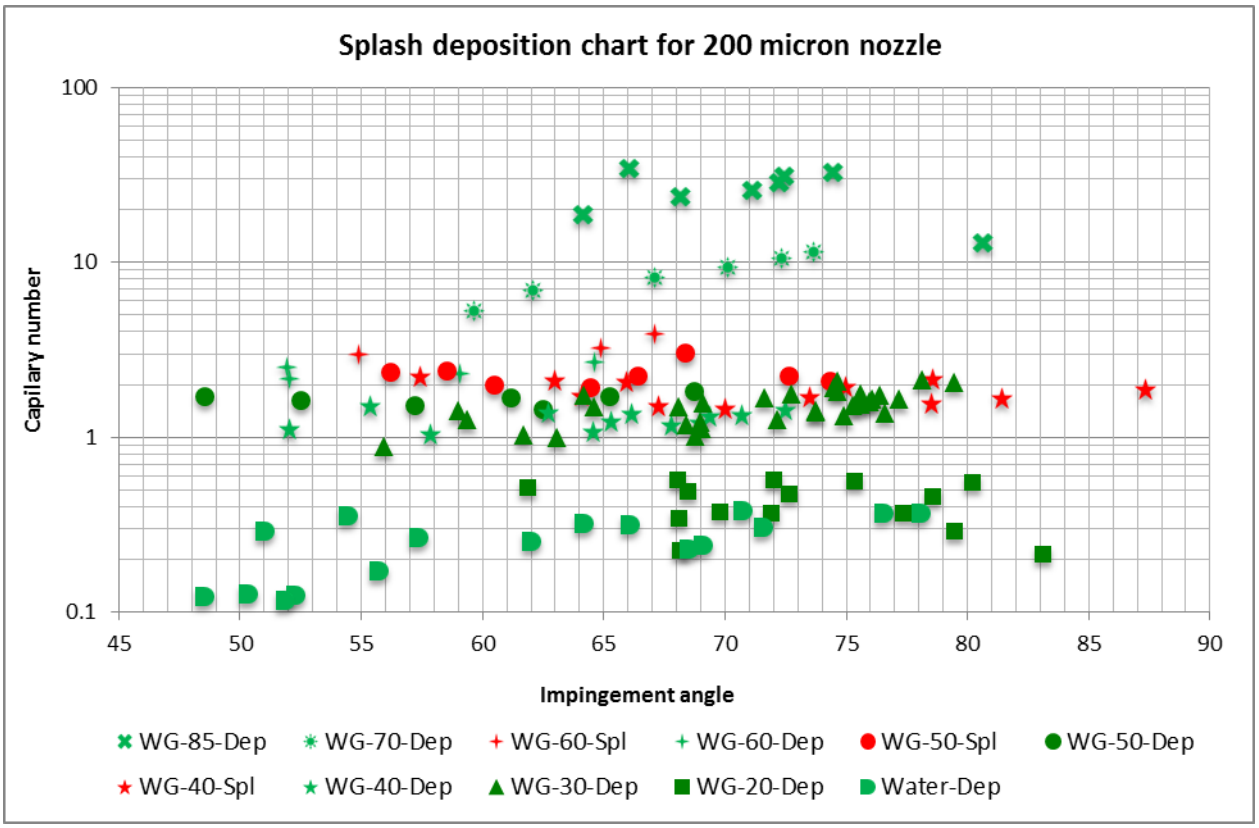

Figure 23 Effect of jet impingement angle and Ca on splash-deposition results of water-glycerin solutions dispensed through a 200 micron nozzle

Figure 23 clearly illustrates that no splash occurs when Ca ≤ 1 and Ca ≥ 5, but splash does occur when 1 ≤ Ca ≤ 5. One can also conclude that jet deposition is governed most significantly by the Capillary number value. In the deposition/splash zone there is almost negligible dependence on the impingement angle. In the region where splash points are located (i.e. points between 1 ≤ Ca ≤ 5), it is reasonable to say that the effect of the jet impingement angle is negligible compared to effect of the Capillary number.

This trend - deposition for low and high viscosity liquids, but splash for mid-range viscosity liquids - was consistent with the 400 micron nozzle as well. However, despite this fact the range of viscosity at which splash occurs increased; for the 200 micron nozzle the viscosity range was from WG-40 to WG-65, but for the 400 micron nozzle it changed from WG-35 to WG-75.

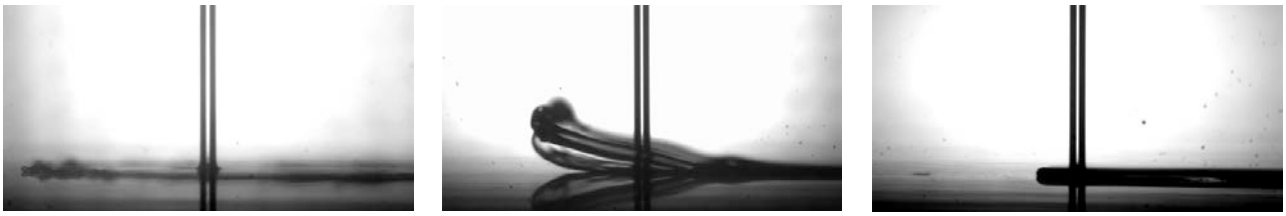

Figure 24 Impingement of water (left), WG-75 and WG-85 (right) jets (generated from a 400 micron nozzle) with a jet speed of 15 m/s on a surface moving from left to right at 5 m/s.

Figure 24 shows that water and WG-85 jets deposit on the moving surface, and WG-75 jets splash at jet and surface speeds of 15 m/s and 5 m/s respectively. From Figures 20 and 23 it can be understood that the splashing of jets of mid-ranged viscosities is not limited to only 200 micron jets but to other jets as well. It is also noticeable, similar results with 200 micron nozzle, from the above figure that the spread radius decreases as the viscosity of the liquid increases. Upon calculating the lamella thickness using the spread radius we found that the lamella thickness increases as the viscosity of the liquid increases.

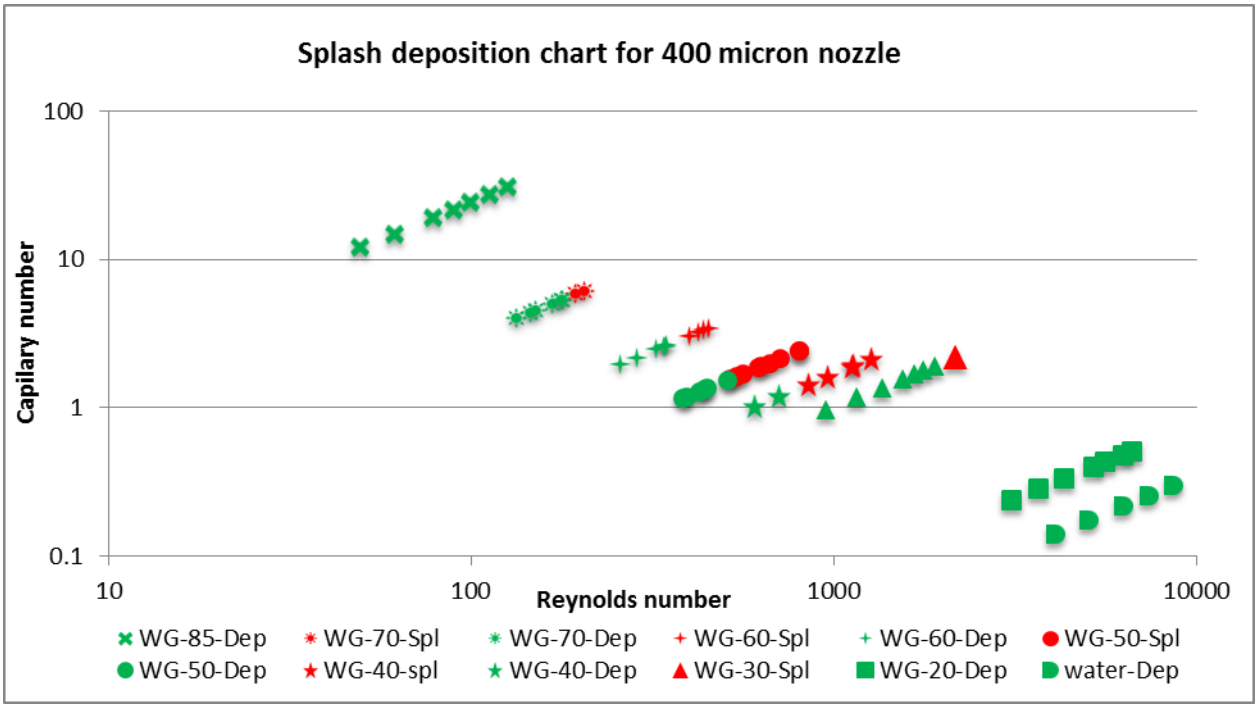

Figure 25 Effects of Re and Ca on splash-deposition results of water-glycerin solutions using a 400 micron nozzle

Figure 25 shows results obtained for experiments conducted with a 400 micron nozzle using the same water glycerin mixtures used for the 200 micron nozzle. It can be observed from the plot that splash does not take place when a low Capillary number is accompanied with a high

Reynolds number, and when a high capillary number accompanies a low Reynolds number. Splash does occur, however, when the Capillary and Reynolds numbers are at a medium level. Comparing the above plot with results for the 200 micron nozzle (Figure 21) we can infer that although splashing starts for the same liquids generated through both nozzles, the range of splashing for the 400 micron nozzle is clearly larger than the range for the 200 micron nozzle.

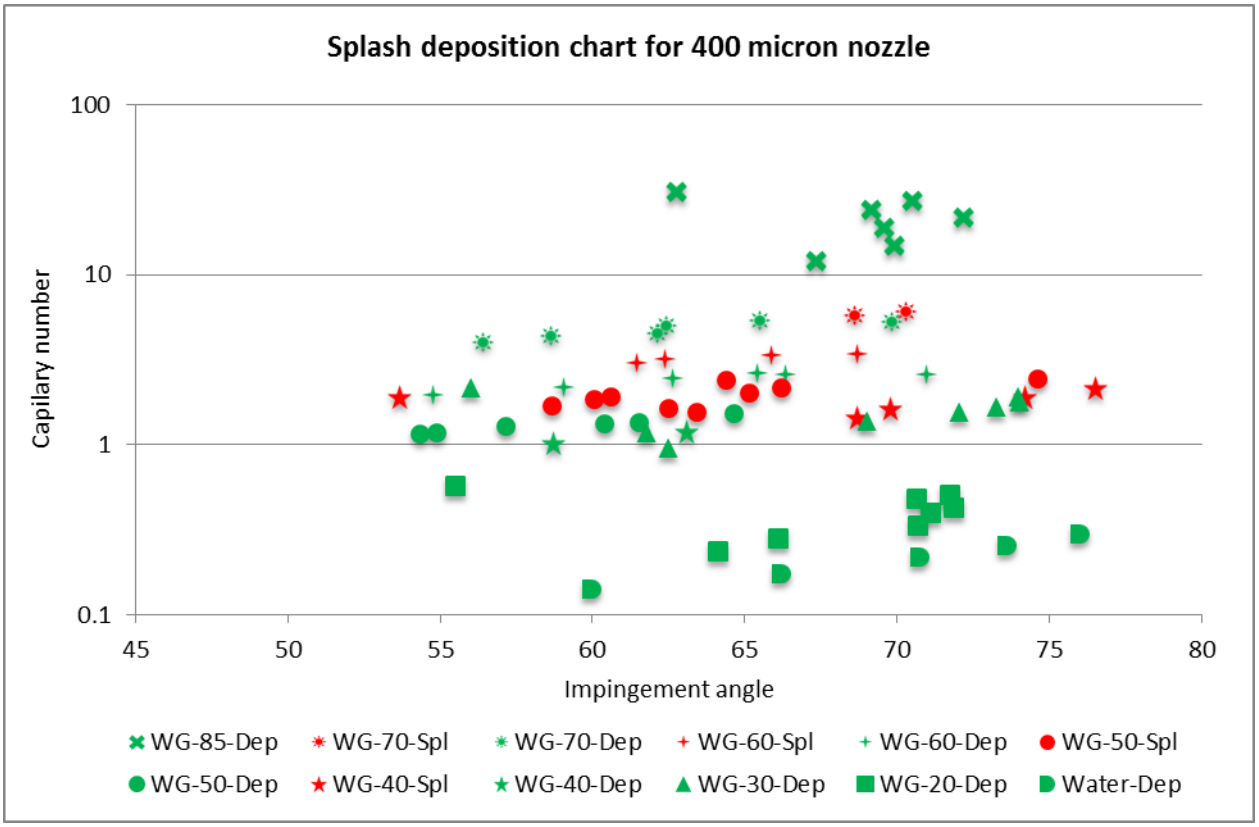

Figure 26 Effect of the jet impingement angle and Ca on splash-deposition results of water-glycerin solutions using a 400 micron nozzle

Figure 26 clearly shows that both splash and deposition results are determined by the Capillary number value. The plot also reveals that the jet impingement angle has an almost negligible effect on splash and deposition. Similar behavior has been observed with the 200 micron nozzle (Figure 23).

Figures 23 and 26 illustrate that under certain conditions both splash and deposition values are very close, and in some cases the values actually overlap. This occurs because the splash/deposition of a liquid jet on a moving surface depends on several non-dimensional numbers such as the Reynolds number, Capillary number, Ohnesorge number, surface roughness ratio and jet impingement angle. The above plots, however, are simply two-

dimensional projections of a multi-dimensional plot. While one jet may splash due to a high Reynolds number, and another jet may deposit as a result of a low Reynolds number, these different results may occur in the presence of similar Capillary number values and jet impingement angles. This causes both the deposition and splash points to overlap, which can generate confusion when analyzing results. Regardless of this behavior we can still infer from the above plots that the jet impingement angle has a weaker effect on jet impingement outcomes than the Capillary number does.

We also conducted experiments with other liquids of a similar viscosity range to make sure that this behavior did not occur due to an anomaly in water-glycerin solutions. We used water-propylene glycol solutions of different percentages to match the viscosity of the water-glycerin solutions. Propylene glycol is easily soluble in water, and upon 24 hours of mixing it does not degrade over time. The rheometry showed that the water and propylene glycol mixture is purely Newtonian with a surface tension of at least half of that of water. The experiments were conducted with a 200 micron nozzle and only with liquids which had a viscosity range of WG-40 to WG-65. The results obtained from the water-propylene glycol experiments were consistent with the water-glycerin results.

Figure 27 Impingement of WPG-05 (left), WPG-50 and WPG-75 (right) jets (generated from a 200 micron nozzle) with a jet speed of 15 m/s on a surface moving from left to right at 5 m/s.

Comparing Figures 20, 24 and 27 we can infer that water-glycerin liquid jet and other liquids with viscosities from 7 mPas – 18 mPas produce similar splash behaviour. As well, it is interesting to note that although the surface tension of the water-propylene glycol solutions is almost 40% lower than that of the water-glycerin solutions, splashing behaviour remains constant.

3.4 Mathematical explanation for splash of liquid jets of mid-range viscosities

The splash and deposition of a liquid jets are related to several flow and fluid properties (jet and surface velocities, density, surface tension, viscosity and elasticity). For Newtonian liquid jets we observed that low viscosity liquid jet deposits on the surface and when viscosity of fluid

increases it starts to splash and finally at relatively higher viscosity it deposits again. The results were very interesting because previously Keshavarz [28] have shown increase in the viscosities, always lead to better chances of deposition. After careful observation of their results we found that viscosity range in which they [28] conducted their experiments and reported their results were already in higher end of our viscosity range. Our results also support that premise.

After analyzing the splash dynamics we observed that as the viscosity of the liquids increase the lamella thickness created by impinging jets also increase. We found by that a square root relation between lamella thickness and liquid viscosity exits and it is valid for liquids used in this study. It was also observed from high speed videos of the experiments that lift of the lamella (inception of splash) is related to thickness of the lamella and inertia of the jet. In other words the splash is closely related to the forces acting on the lamella.

There are three major forces acting on the lamella; inertia, viscous and surface tension forces. The inertia force comes from the jet velocity and the density of the liquid. It tends to break the lamella causing the splash and both viscous and surface tension forces acts as resistance force and keep to lamella attached to the target surface. The forces on lamella depend on both velocity and thickness of the lamella, and fluid properties. As the lamella thickness grows due to increase in fluid viscosity, the area of the surface open to air decrease making surface tension forces smaller. Increase in thickness also decreases the shear rate but due to increase in viscosity overall viscous forces increases. Therefore with increase in viscosity, lamella thickness increases, surface tension forces decreases and viscous forces increases.

After plotting the magnitude of the overall stresses on the lamella, we found that there is certain viscosity range where the overall force becomes negative i.e. inertia force becomes larger than combined viscous and surface tension force, causing jet to splash.

3.4.1 Comparison of forces/stresses on lamella

The magnitude of the stresses on lamella has been calculated with formulations mentioned below. The thickness of the lamella and the velocity in the expression below has been calculated from equation 3.2 and equation 3.4.

$$surface\ tension\ stress \sim \frac{\sigma}{T} \tag{3.6}$$

$$Shear\ stress \sim \frac{\mu V_{rel}}{T} \tag{3.7}$$

$$Inertial\ stress \sim \rho \cdot V_{rel}^2 \quad (3.8)$$

The results shown in figures 28 and 29 are obtained with 200 micron nozzle and jet and surface velocity = 15 and 10 m/s respectively. Figure 28 clearly shows that as the percentage of glycerin increases the inertial stress increases (because of increase in density), shear stress also increase (because of rapid increase in viscosity) but surface tension stress decrease. Because of this the combined resistance forces (viscous + surface tension force) first decreases and then increases.

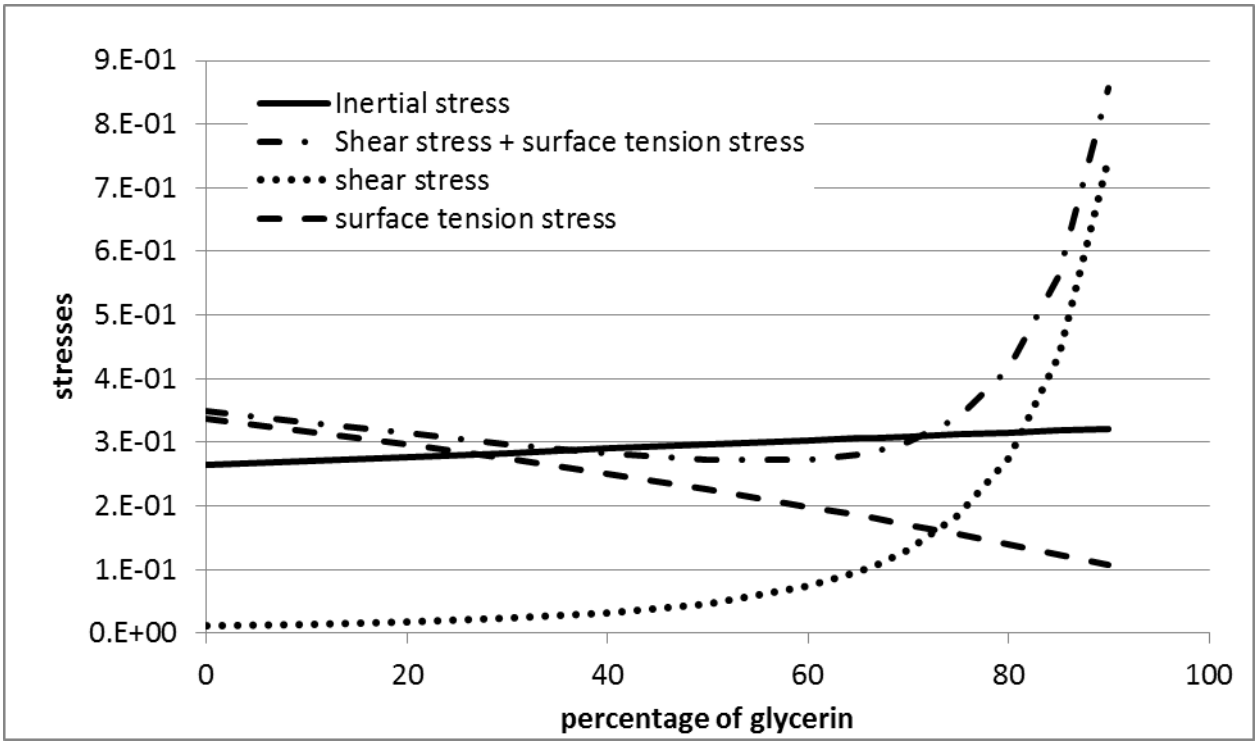

Figure 28 Inertial, shear and surface tension stresses on the lamella

The above figure also shows that between 35 to 75 percentages of glycerin the inertial stress is higher than resistance stresses.

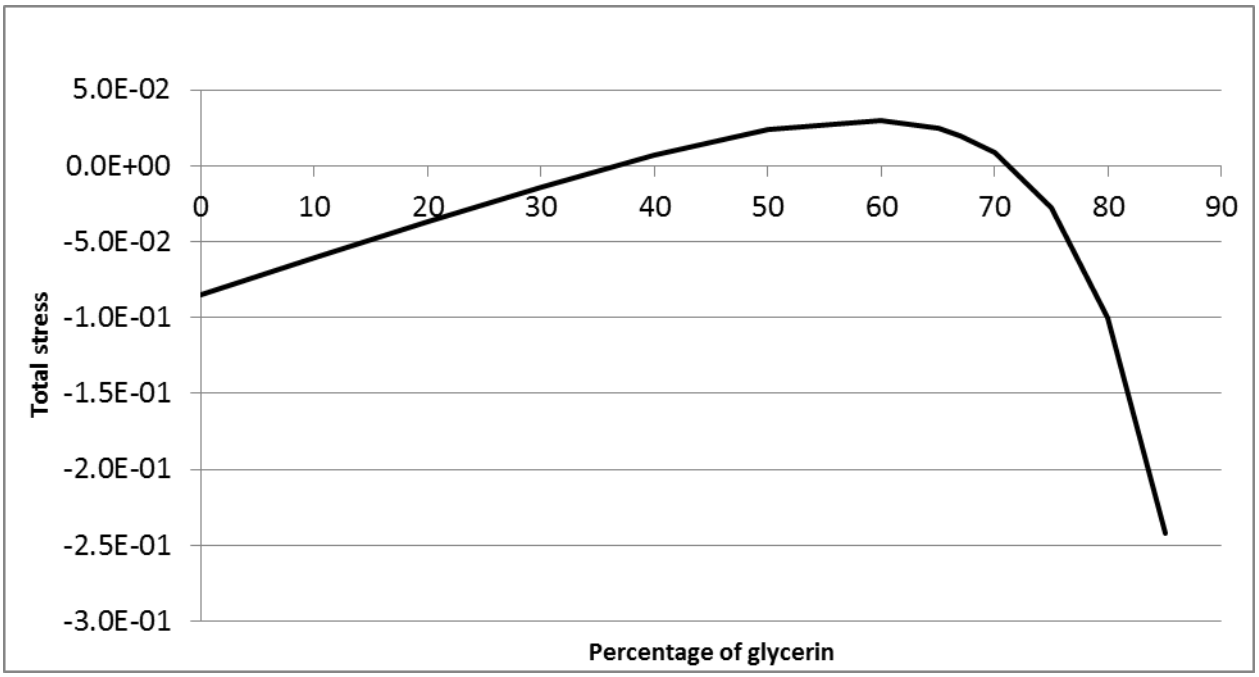

Figure 29 Total stress on the lamella

Figure 29 illustrate the total stress on the lamella and between 35 to 75 percentages of glycerin it becomes positive making inertial stress higher than the resistance stress. This is the region where we have observed the splash even at 15 m/s of relative jet velocity.

3.5 Summary

This study has experimentally investigated the impaction of a free-surface jet of Newtonian fluid on a moving surface. In particular, the study has focused on the effect of jet and surface velocity, and fluid properties on jet splash/deposition characteristics. Several different Newtonian fluids with varying viscosity and surface tension values were tested, including water-glycerin and water-propylene glycol solutions. High-speed imaging was used to visualize splash dynamics on the moving surface. Two nozzles with 200 micron and 400 micron diameters were used to conduct this experiment. The viscosity, surface tension, jet velocity and surface velocity for these experiments ranged from 1-90 mPas, 35-72 mN/m, 5-40 m/s and 5-15 m/s respectively. The combination jet velocity, surface velocity and fluid properties gave a wide range of Re (10 – 8000) and We (200 – 400).

The key findings of these experimental studies are:

- Both the jet speed (normal speed) and surface speed (tangential speed) play a role in the splash or deposition of a jet on a surface.

- Both the surface tension and viscosity of a liquid are important in counter balancing the inertial force of the jet.
- The effect of the jet impingement angle is negligible compared to the jet relative velocity and fluid properties.
- The jet impingement spread radius of low viscosity liquids is higher than that of high viscosity liquids.
- The lamella thickness increases as the viscosity, surface speed and jet diameter increase, but decreases with an increase in jet velocity.

Chapter 4 - Experiments using KELTRACK® Solutions

4.1 Introduction

KELTRACK® is a liquid friction modifier product produced by Kelsan Technology Corporation. It is dark grey, water-based liquid with solid particle and polymer suspensions. As the liquid is mixed thoroughly, the macro suspensions are not visible to the naked eye. This KELTRACK® liquid is prone to solidification if left exposed to open air for long periods of time. Field experiments conducted by Kelsan report that application of this liquid reduce locomotive fuel consumption by 6-8%. The product also reduces the rate of wheel and track wear, as well as noise levels in locations surrounding rail tracks.

During this graduate research study we conducted experiments using Newtonian, shear thinning and elastic liquids of constant viscosities. Results showed that increasing the viscosity, elasticity and consistency constant (k) of liquids inhibits splash. It was our growing interest that motivated us to conduct experiments with liquids that exhibited both strong shear thinning and large relaxation times. From this experimental study we were able to analyze the combined effects of both shear thinning and elasticity on the splash-deposition characteristics of the impinging jet.

4.2 Liquids prepared

Rheometry tests show that KELTRACK® is a non-Newtonian liquid, exhibiting significant shear thinning and elasticity but minimal yield stress. Three samples of KELTRACK® were obtained from Kelsan Technology Corporation to perform these experiments. The first solution, KELTRACK® normal Hi-rail, shows a 1000 cP shear viscosity under a 20 revolutions/second shear rate. The second solution possesses a 50% lower viscosity than KELTRACK® normal Hi-rail, and the third solution is 50% higher in viscosity than KELTRACK® normal Hi-rail. The same experimental setup along with a 400 micron nozzle (described in Chapter 2 and 3) was used in these experiments.

4.3 Results and discussions

4.3.1 Rheometry of the liquids

We performed rheometry, mass flow rate and splash-deposition experiments. The rheometry experiment involved measuring both the relaxation times and shear viscosities of the liquids. Shear viscosity was measured using a Bohlin CS 10 rheometer with a serrated parallel plate setup. Shear viscosity measurements showed a very low yield stress value for all three liquids.

The relaxation time was measured using a Kinexus Rheometer from Malvern®. 1 Pa shear stress was applied to the samples in the frequency range of 1 - 50 Hz. The relaxation time was obtained by locating the intersection point of the shear storage modulus (G') and shear loss modulus (G'') curves. For some elastic liquids there can be more than one intersection point, meaning that the liquid has more than one relaxation time. The three liquids that we observed however only had one intersection point and, hence, only one relaxation time.

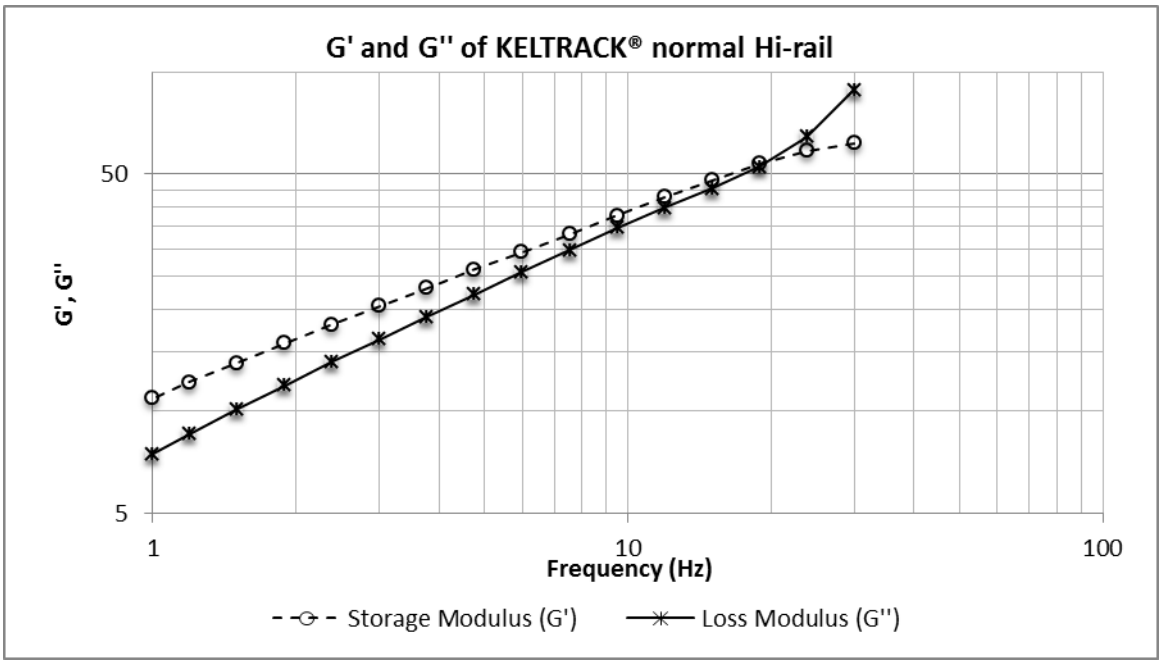

Figure 30 Storage and Loss moduli of the KELTRACK® Normal Hi-rail solution

Figure 30 shows that the shear storage modulus (G') and shear loss modulus (G'') intersects at 19.83 Hz. The relaxation time is calculated using the below expression,

$$Relaxation\,time\,(\lambda) = \frac{1}{frequency}$$

The units for relaxation time and frequency are *sec* and *Hz* respectively.

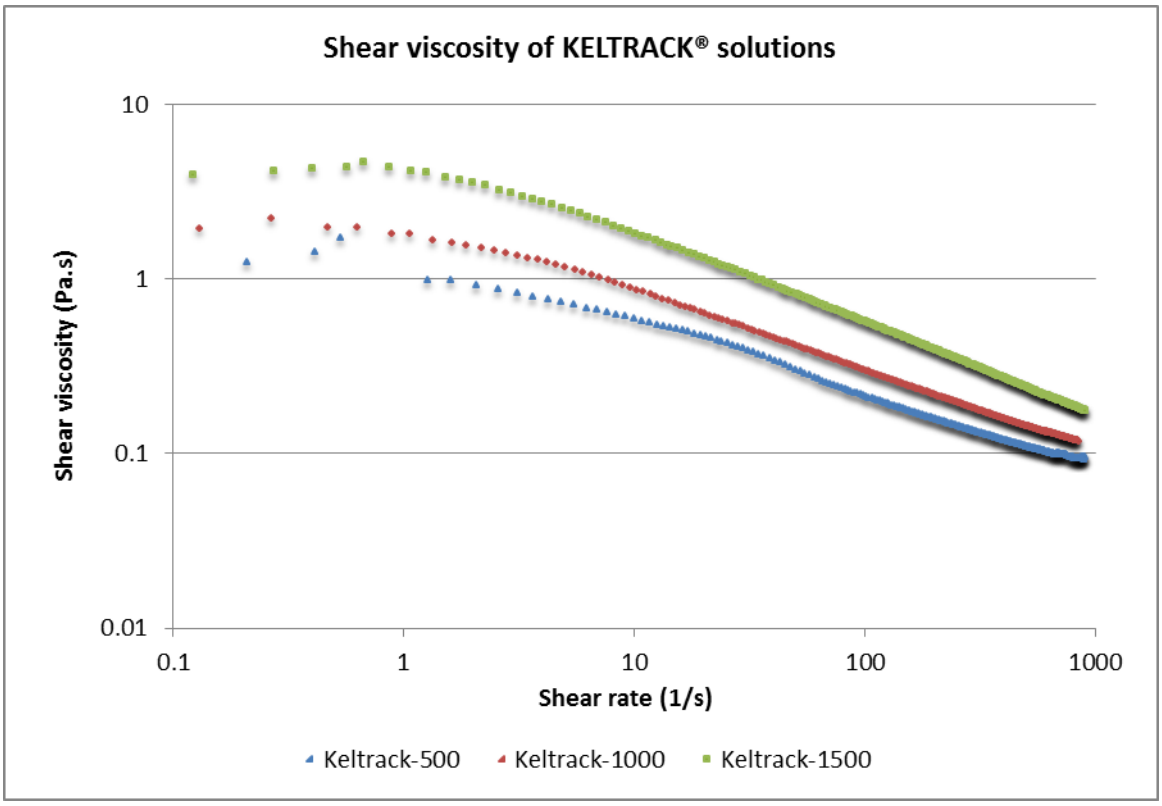

Figure 31 Shear viscosities of KELTRACK® solutions

Figure 31 clearly shows that the shear viscosity of the samples decreases as the applied shear rate increases. Because viscosity levels remain almost constant as shear rates rise from 0.1 - 0.5, the values of yield stress is almost negligible for these liquids. The rheological properties of all three KELTRACK® solutions are listed in Table 6.

Table 6 Rheological properties of KELTRACK® solutions

Product Name	Product Code	Relaxation Time (ms)	Yield Stress (Pa)	Consistency Constant	Power Law Index
Keltrack-500	SS-2096-02-01	50.22	2.866	0.766	0.68
Keltrack-1000	505-HR1-19000	52.82	1.383	1.931	0.58
Keltrack-1500	SS-2096-02-02	83.75	3.014	7.602	0.45

4.3.2 Mass flow rate measurements

The mass flow rates were measured using the same method explained in previous chapters (Chapter 2 and 3). The results presented in Figure 31 show that the mass flow rates for Keltrack-500 and Keltrack-1000 are very close in value. However, when including higher

viscosity solutions in the comparisons (Keltrack-1500), the flow rate curves start to diverge. Flow rate patterns also show that losses are almost negligible due to an increase in viscosity at lower nozzle back pressures; similar mass flow rates were shown for all three liquids. Similar results have been shown in previous chapters.

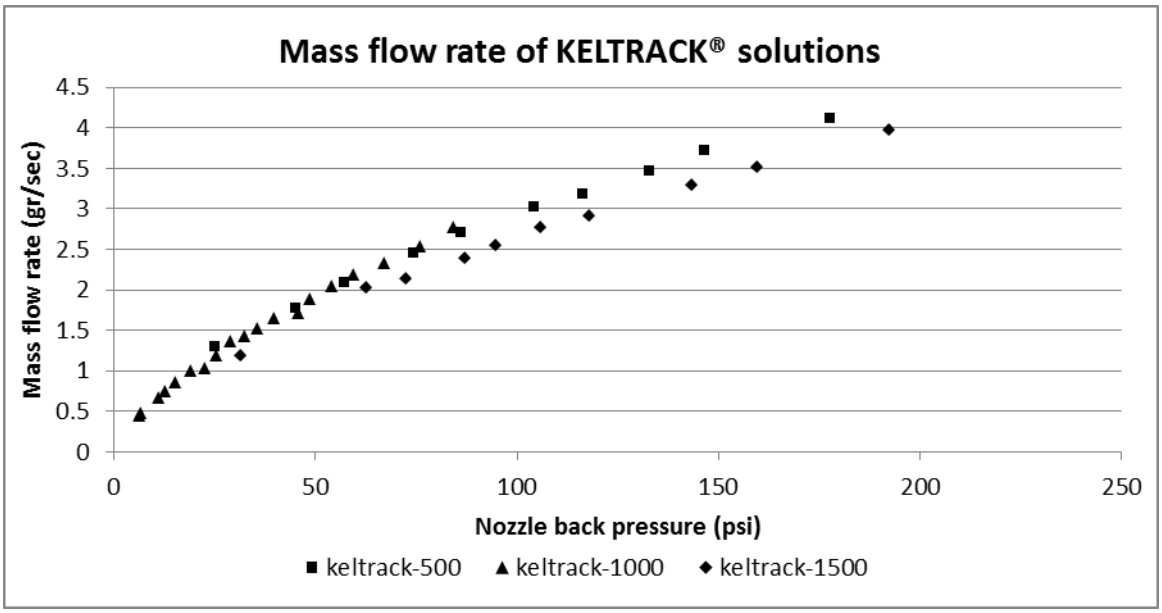

Figure 32 Mass flow rates of KELTRACK® solutions projected through a 400 micron nozzle

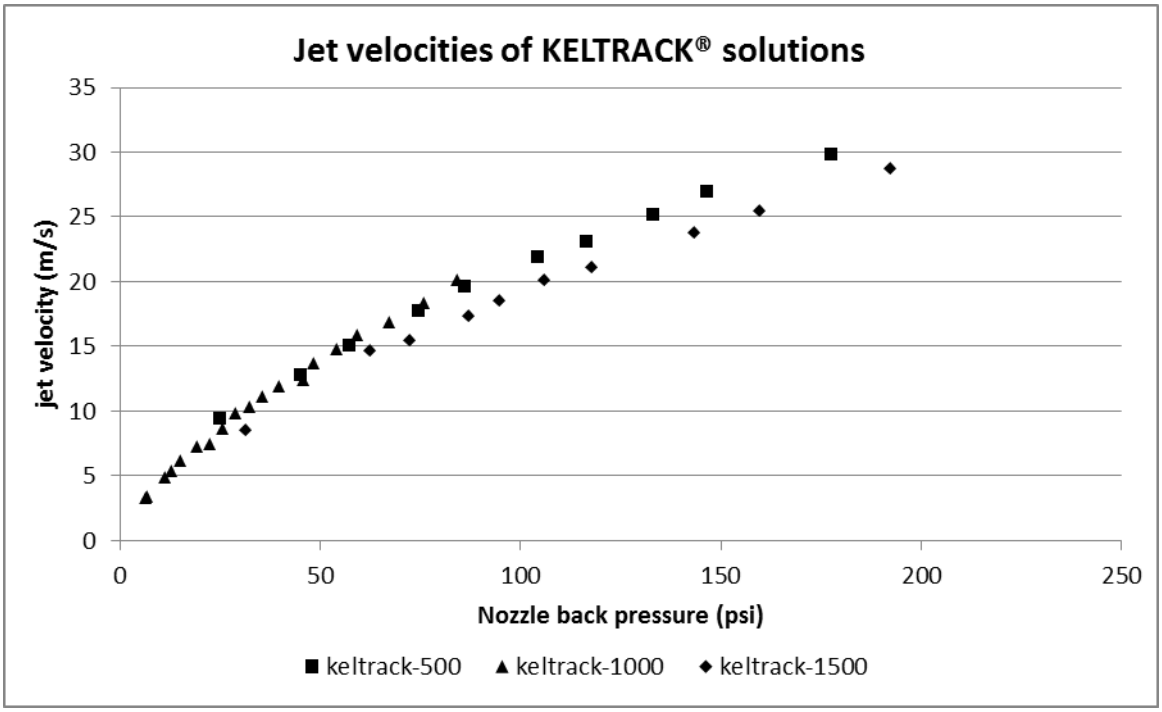

Figure 33 Jet velocities of KELTRACK® solutions projected through a 400 micron nozzle

In order to avoid jet deflection in the presence of a 60-70 km/h crosswind, jet velocity must be sustained at a minimum of 12 m/s. This jet velocity is easily achievable using 400 micron nozzle. Figure 33 shows that under a 60 psi nozzle back pressure, the jet velocity is 15 m/s for all three liquids. It is also worth mentioning that the mass flow rate for a 15 m/s jet velocity is 2.19 g/sec, an application rate that Kelsan Technology Corporation could reasonably adopt.

4.3.3 Splash-deposition experiments

The results of our splash-deposition experiments with all three KELTRACK® solutions revealed that the liquid jet is stable as it exits the nozzle. All instabilities caused by capillary forces and nozzle geometries are negligible here. Figure 34 illustrates that the liquid jet does not exhibit any waviness prior to impacting the surface.

4.3.3.1 Effect of jet and surface speeds

It has been proven that for Newtonian and non-Newtonian liquids, both jet and surface speed play a role in the splash-deposition behavior of a jet impacting a moving surface. To study the effect of surface speed on jet impaction for the three KELTRACK® solutions, we conducted experiments that varied the jet and surface speed separately. Our results show that increasing the jet speed while the keeping surface speed nearly constant changes the impingement outcome from deposition to splash. Similar results were observed when jet speed was kept constant while surface speed was continuously increased.

Though we conducted experiments with all three KELTRACK® solutions, the following images depict results obtained from the KELTRACK® normal Hi-rail (Keltrack-1000) solution only.

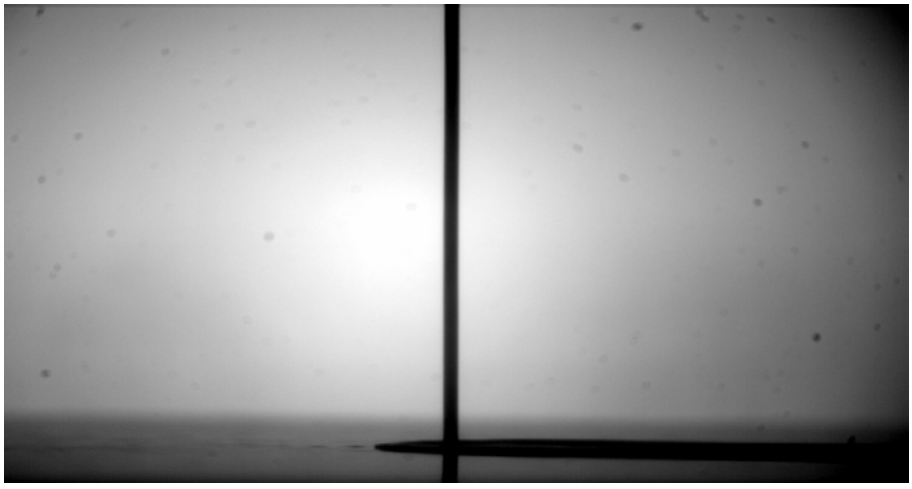

Figure 34 Jet velocity = 27.4, surface velocity = 10.1 m/s

Figure 34 clearly shows that when jet velocity = 27.4 and surface velocity = 10.1 m/s, jets deposit smoothly. There is also no instability along the edges of the lamella (liquid spread on the surface). This demonstrates the effectiveness of high viscosity and elasticity in inhibiting splash. When jet velocity is increased further to 29.7 m/s while keeping the surface velocity at 10.5 m/s however, the jet begins to splash. Although the splash pattern appears vigorous, ligaments and droplets from the lamella do not separate from the surface. The formation of resilient ligaments is related to the high elasticity of the KELTRACK® solutions.

Figure 35 Jet velocity = 29.7, projectile velocity = 10.5 m/s

4.3.3.2 Effect of surface temperature

Because the temperature of a rail track while in operation can vary from 5 - 100°C, and temperature fluctuations can alter fluid properties such as viscosity, surface tension and elasticity, we conducted experiments at elevated temperatures up to 62°C. The experiments were carried out in the vicinity of the splash threshold to study if a change in surface temperature causes any change to the splash threshold. We used the KELTRACK® normal hi-rail (Keltrack-1000) solution and a 400 micron nozzle as the test liquid and nozzle respectively. The experiments were conducted at room temperature, 25°C, 55°C and 62°C. The results show that elevated temperatures do not have a significant effect on splash/deposition results. All three liquids showed deposition at below mentioned velocities.

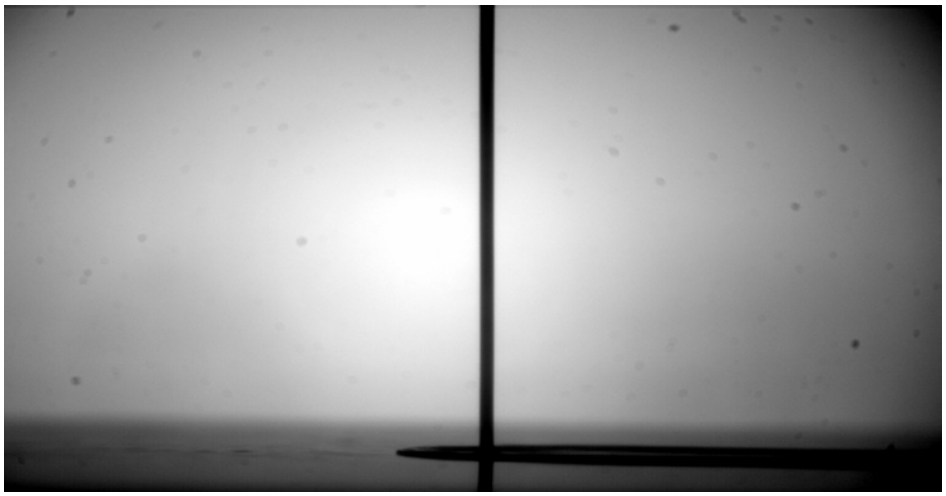

Figure 36 Jet velocity = 26.9, projectile velocity = 6.77 m/s at 55°C surface temperature

Although we did not observe any significant change to the splash threshold due to changing surface temperatures, the lamella (liquid spread) did dry up immediately upon jet impingement. This occurred because the temperature gradient was high enough to evaporate the lamella, since the lamella had a thickness of only a few microns.

4.3.3.3 Effect of shear viscosity and elasticity

As mentioned previously, we used three test liquids to perform these experiments. The names and rheological properties of these liquids are listed in Table 6. Table 7 reports the rheological properties and splash thresholds for each liquid. We obtained the splash threshold for each liquid by conducting experiments where the liquid jet speed was changed while the surface speed was kept constant, and vice versa.

Table 7 Rheological properties and splash thresholds of KELTRACK® solutions

Row	Product Name	Relaxation Time (ms)	Yield Stress (Pa)	Consistency Constant	Power Law Index	Splash Threshold
1	Keltrack-500	50.22	2.866	0.766	0.68	25.5 m/s
2	Keltrack-1000	52.82	1.383	1.931	0.58	32.4 m/s
3	Keltrack-1500	83.75	3.014	7.602	0.45	No splash

While we found the splash threshold for Keltrack-500 and Keltrack-1000, due to limitations in our experimental setup we could not find the splash threshold for Keltrack-1500. Though the Keltrack-1500 liquid jet still showed deposition at a relative jet speed of 35 m/s, we could not

increase jet velocities any further than this. Hence we did not observe any splash threshold for this liquid.

Rows 1 and 2 of Table 7 show that keeping the liquid elasticity constant (at very close relaxation time values) while increasing the liquid viscosity increases the splash threshold. The splash threshold increases from 25.5 - 32.4 m/s when the viscosity is nearly doubled. Rows 2 and 3 show that increasing both the elasticity and viscosity of the liquid also increase the splash threshold. In other words, increasing liquid viscosity and elasticity aids in inhibiting splash.

4.4 Summary

An experimental study of jet impingement on a moving surface was conducted by means of high speed imaging. Three samples of KELTRACK® liquid friction modifier were used as test liquids. KELTRACK® is a non-Newtonian fluid that exhibits both shear thinning and elastic behavior. The relaxation time and consistency constant of the liquids ranged from 50 – 80 ms and 0.76 – 7.60 respectively. The jet and surface speed of this study ranged from 5 – 35 m/s and 5 – 15 m/s respectively. A 400 micron nozzle dispensed the liquid jet, after which the jet impinged on the surface from a height of 10 cm.

The key findings of this experimental study are:

- Both jet and surface speed play a role in the splash-deposition characteristics of the jet.
- Increasing liquid elasticity and viscosity both increases the splash threshold and stabilizes the liquid jet upon exiting the nozzle.
- The temperature of the surface has a negligible effect on the splash threshold of the KELTRACK® solutions.
- When jet splash does take place, ligaments remain attached to the lamella due to high elastic forces.

Chapter 5 - Conclusions and Recommendations for Future Works

5.1 Conclusions

A systematic study of jet impact on moving surfaces was conducted with both Newtonian fluids and non-Newtonian fluids to study effects of viscosity, surface tension, jet diameter, jet and surface velocities, and surface temperature on splash characteristics of jet impingement. A high speed camera was used to capture the images of the jet interacting with a moving surface. The liquid jet was generated from nozzles with internal diameter 200, 400 and 648 micron. The results obtained from these experiments provided better insight into jet impingement on a stationary and a moving surface. All the conclusions drawn into this research work has been reported below in form of categories.

5.1.1 Conclusions for non-Newtonian fluids

Seven different samples of non-Newtonian liquids (Carbopol and water solutions) with varying yield stress, consistency constant and power-law indices were tested. The yield stress, consistency constant, power-law index, jet velocity and surface velocity for these experiments ranged from 10-90 Pa, 6-85, 0.28-0.36, 5-40 m/s and 5-15 m/s respectively. The combination jet velocity, surface velocity and fluid properties gave a wide range of Re (1 – 100), Od (0.01-0.1) and We (1 – 120).

The key findings of these experimental studies are:

- Both jet speed (normal speed) and surface speed (tangential speed) play roles in the splash or deposition of the jet on a surface. By keeping the surface speed constant and increasing the jet speed the impingement results changes from deposition to splash. Same result was obtained when jet speed was kept constant and surface speed was increased. The resultant velocity to get splash for individual liquids was almost similar with both the approaches.
- Both the yield stress and consistency constant of the liquids are important in balancing the inertial force of the jet. By increasing the yield stress and consistency constant we were able to get the deposition at even higher resultant velocities.
- The effects of the jet impingement angle are negligible compared to the effects of the jet relative velocity and fluid properties.
- The surface tension forces are dominant compared to the viscous forces only at low Weber numbers.

5.1.2 Conclusions for Newtonian fluids

Several different Newtonian fluids with varying viscosity and surface tension values were tested, including water-glycerin and water-propylene glycol solutions. The liquid jet was generated with 200 micron and 400 micron diameters nozzles. The viscosity, surface tension, jet velocity and surface velocity for these experiments ranged from 1-90 mPas, 35-72 mN/m, 5-40 m/s and 5-15 m/s respectively. The combination jet velocity, surface velocity and fluid properties gave a wide range of Re (10 – 8000) and We (200 – 400).

The key findings of these experimental studies are:

- Both the jet speed (normal speed) and surface speed (tangential speed) play a role in the splash or deposition of a jet on a surface.
- Both the surface tension and viscosity of a liquid are important in counter balancing the inertial force of the jet. The effect of surface tension was observable only for low viscosity (Water to Water-70%+glycerin-30%) jets and for high viscosity fluid effects of viscosity was dominant.
- The jet impingement spread radius of low viscosity liquids is higher than that of high viscosity liquids.
- The lamella thickness increases as the viscosity, surface speed and jet diameter increase, but decreases with an increase in jet velocity. As the viscosity of the liquids increase the fluid decelerates quickly and at shorter distance from impingement point making the spreading smaller and lamella thickness higher.
- The effect of the jet impingement angle is negligible compared to the jet relative velocity and fluid properties.

5.1.3 Conclusions for KELTRACK solutions

Three samples of KELTRACK® liquid friction modifier were used as test liquids. KELTRACK® is a non-Newtonian fluid that exhibits both shear thinning and elastic behavior. A 400 micron nozzle was used to generate the liquid jet. The relaxation time and consistency constant of the liquids ranged from 50 – 80 ms and 0.76 – 7.60 respectively. The jet and surface speed of this study ranged from 5 – 35 m/s and 5 – 15 m/s respectively. A 400 micron nozzle dispensed the liquid jet, after which the jet impinged on the surface from a height of 10 cm.

The key findings of this experimental study are:

- Both jet and surface speed play a role in the splash-deposition characteristics of the jet.
- Increasing liquid elasticity and viscosity both increases the splash threshold and stabilizes the liquid jet upon exiting the nozzle.
- The temperature of the surface has a negligible effect on the splash threshold of the KELTRACK® solutions.
- When jet splash does take place, ligaments remain attached to the lamella due to high elastic forces.

5.2 Strength and limitation of thesis research

The results obtained from this research work have both scientific and practical applications. There is very little known about a jet impingement on a moving surface that makes this research work one of its kinds. The study of effects of individual fluid and flow properties and also combined effects of some of fluid properties have not been conducted in detail previously for jet impingement on a moving surface. Keshavarz [28] reported that for a Newtonian jet impinging on a moving surface the critical Reynolds to get splash is 350 but prove that it is possible to get depositions even at Re = 8000. We also have been able to study the combined effects of both shear thinning and elasticity on outcome of jet impingement. The results obtained here can be applied to jet impingement on a stationary or a slow moving target.

All the experiments in this research work were done with a slow moving target therefore these results may not be applicable to high speed moving targets. The thickness and velocity profiles of fluid on the target surface are also not possible to estimate with our current experimental setup that makes our results little bit off from actual numbers. But qualitatively the results are very promising.

5.3 Potential applications of research findings

The results obtained in this research work can be applied to several industrial applications. In curtain coating industry it is very necessary to provide uniform coating without wasting too much of product. By putting several airless nozzles perpendicular to curtain speed direction proper coating can be achieved. This will also ensure minimal wasting of the product if application rate is kept in deposition range.

The research findings from this research work can also be applied for understanding hydrodynamics section of heat transfer through liquid jet impingement. Another use for liquid jet

impingement is the application of liquid friction modifier (LFM) to railroad tracks for friction control. Currently the LFM is applied with air blast atomization which has very poor transfer efficiency but if airless jet impingement is used it can improve the efficiency considerably.

5.4 Recommendations for future works

The experiments conducted in research work have provided some very promising results for using airless jet impingement in rail road industry for utilization of Liquid Friction Modifiers. Therefore there is need to explore this area further and find the best way to harness this technology. Some of the works that can be useful for both industry and academia are listed below:

- All the experiments in this research work have been conducted in academic setup therefore neglecting any change in surrounding air, pressure or temperature. Therefore the effects of surrounding air need to be studied. It can be achieved by performing experiment inside a vacuum chamber at reduced air pressure. This will definitely give an idea regarding effects of the air.
- The current setup does not enable us to add crosswind or vibration, and associated boundary layer effects that may happen in the field for the impacting rail surface. These effects may multiply at high speed application therefore a more elaborate experimental setup can be designed to conduct these experiments.
- Although effects of individual fluid properties (surface tension, viscosity and elasticity) have be studied, it is desirable to study combined effects of surface tension and elasticity or viscosity and elasticity because KELTRACK® or any other industrial liquids have elasticity and viscosity together.
- These experiments have been conducted with slow moving targets and results obtained are very promising but due to upsurge interest in high speed trains, further studies for the application of the same airless nozzle for higher train/jet speeds can be an interesting field for both industrial and academic challenges.
- It will be useful to the amount of the liquid adhering to the target surface in case of the splash of the liquid jet after impingement. This will also provide logical insight into the transfer efficiency of this mode of application.

Bibliography

[1] Cotter, J., Eadie, D.T., Elvidge, D., Hooper, N., Robert, J., Makowsky, T., and Liu, Y., 2005. Top of Rail Friction Control : Reductions in Fuel and Greenhouse Gas Emissions. In: Proc. Of the 2005 Conference of the International Heavy Haul Association (Rio de Janeiro), pp. 327-334.

[2] Li, L.K.B., Dressler, D.M., Green, S.I., Davy, M.H., and Eadie, D.T., 2009. Experiments on Air-Blast Atomization of Viscoelastic Liquids, Part 1: quiescent Conditions. Journal of Atomization and Sprays, 19:157-190.

[3] Dressler, D.M., Li, L.K.B., Green, S.I., Davy, M.H., and Eadie, D.T., 2009. Newtonian and Non-Newtonian Spray Interaction with a High-Speed Moving Surface. Journal of Atomization and Sprays, 19:19-39.

[4] Li, L.K.B., Green, S.I., Davy, M.H., and Eadie, D.T., 2010, Air-blast atomization of viscoelastic liquids in a cross-flow, Part 1: Spray Penetration and Dispersion, accepted for publication in Journal of Atomization and Sprays.

[5] Li, L.K.B., Green, S.I., Davy, M., and Eadie, D.T., 2010, Air-blast atomization of viscoelastic liquids in a cross-flow, Part 2: Droplet velocities, accepted for publication in Journal of Atomization and Sprays.

[6] Yarin, A.L., 2006, Drop Impact Dynamics: Splashing, Spreading, Receding, Bouncing, Annual Review of Fluid Mechanics, 38:159-192.

[7] Povarov, O.A., Nazarov, O.I., Ignat'evskaya, L.A., and Nikol'Skii, A.I., 1976, Interaction of drops with boundary layer on rotating surface, Journal of Engineering Physics, 31:1453-1456.

[8] Fathi, S., Dickens, P., and Fouchal, F., 2010, Regimes of droplet train impact on a moving surface in an additive manufacturing process, Journal of Material Processing Technology, 210:550-559.

[9] Bird, J., Tsai, S., Stone, H., (2009), Inclined to splash: triggering and inhibiting a splash with tangential velocity. New Journal of Physics, 11:063017.

[10] Nigen, S. (2005). Experimental investigation of the impact of an (apparent) yield-stress material. Atomization and Sprays, 15(1), 103–117.

[11] German, G., & Bertola, V. (2009). Impact of shear-thinning and yield-stress drops on solid substrates. Journal of Physics-Condensed Matter, 21:375111

[12] German, G., & Bertola, V. (2010). The spreading behaviour of capillary driven yield-stress drops. Colloids and Surfaces a-Physicochemical and Engineering Aspects, 366, 18–26.

[13] Saidi, A., Martin, C., & Magnin, A. (2010). Influence of yield stress on the fluid droplet impact control. Journal of Non-Newtonian Fluid Mechanics, 165, 596–606.

[14] E.J. Watson (1964), The radial spread of a liquid jet over a horizontal plane, J. Fluid Mech., 20, 481–495.
[15] V.E. Nakoryakov, B.G. Pokusaev, E.N. Troyan (1978), Impingement of an axisymmetric liquid jet on a barrier, Int. J. Heat Mass Transfer, 21, 1175–1184.
[16] T. Azuma, T. Hoshino (1984), The radial flow of thin liquid film, Trans. Jpn. Mech. Engrs., 50, 974–1136.
[17] J. Stevens, B.W. Webb (1993), Measurements of flow structure in the radial layer of impinging free-surface liquid jets, Int. J. Heat Mass Transfer, 36 (15), 3751–3758.
[18] Yu. A. Buyevitch, V. A. Ustinov (1994), Hydrodynamic conditions of transfer processes through a radial jet spreading over a flat surface, Int. J. Heat Mass Transfer, 37 (1), 165–173.
[19] Y. Pan, J. Stevens, B.W. Webb (1992), Effect of nozzle configuration on transport in the stagnation zone of axisymmetric, impinging free surface liquid jets. Part 2-Local heat transfer, J. Heat Transfer, 114, 880–886.
[20] T. Bohr, P. Dimon, V. Putkaradze (1993), Shallow water approach to the circular hydraulic jump, J. Fluid Mech., 254, 635–648.
[21] D.A. Zumbrunnen (1991), Convective heat and mass transfer in the stagnation region of a laminar planar jet impinging on a moving surface, J. Heat Transfer, 113, 563–570.
[22] D.A. Zumbrunnen, F.P. Incropera, R. Viskanta (1992), A laminar boundary layer model of heat transfer due to a nonuniform planar jet impinging on a moving plate, Warme und Stoffubertragung, 27, 311–319.
[23] H. Chattopadhyay, S.K. Saha (2003), Turbulent flow and heat transfer from a slot jet impinging on a moving plate, Int. J. Heat Fluid Flow, 24, 685–697.
[24] Bush, J. W. M., Aristoff, J. M., Hosoi, A. E. (2006), An experimental investigation of the stability of the circular hydraulic jump. Journal of Fluid Mechanics, 558, 33.
[25] Gradeck, M., Kouachi, A., Dani, A., Arnoult, D., Borean, J. (2006), Experimental and numerical study of the hydraulic jump of an impinging jet on a moving surface. Experimental thermal and fluid science, 30(3), 193-201.
[26] Roisman, I. V., Horvat, K., Tropea, C. (2006), Spray impact: Rim transverse instability initiating fingering and splash, and description of a secondary spray. Physics of Fluids, 18(10), 102104.
[27] Li, R., Ashgriz, N. (2006), Characteristics of liquid sheets formed by two impinging jets. Physics of Fluids, 18(8), 087104.
[28] Keshavarz, B., 2011, Newtonian and elastic liquid jet interaction with a moving surface, M.A.Sc. Thesis, UBC.

[29] Dressler, D.M., 2006, An experimental investigation of Newtonian and non-Newtonian spray interaction with a moving surface, M.A.Sc. Thesis, UBC.

[30] Suh, H. K., Lee, C. S. (2008), Effect of cavitation in nozzle orifice on the diesel fuel atomization characteristics. International journal of heat and fluid flow, 29(4), 1001–1009.

[31] Park, S., Suh, H. (2007), Effect of Cavitating Flow on the Flow and Fuel Atomization Characteristics of Biodiesel and Diesel Fuels - Energy & Fuels (ACS Publications). Energy and Fuels.

[32] Nguyen, Q. D., Boger, D. V. (1992), Measuring the Flow Properties of Yield Stress Fluids. Annual Review of Fluid Mechanics, 24(1), 47–88.

[33] Eadie, D.T., Bovey, E., and Kalousek, J. (2002), The role of friction control in effective management of the wheel/rail interface, Railway Technical Conference, November 2002.

[34] Eadie, D.T., and Kalousek, J. (2001), Spray it on, Let'em Roll, Railway Age.

[35] Chiddick, K.S., and Eadie, D.T. (1999) Wheel/Rail Friction Management Solutions, Proceedings of the 14th Int. Conference on Current Problems in Rail Vehicles, PRORAIL 1999, Prague, October 1999, pp. 167-173.

Appendices

A - Effect of static contact angles

A.1 Test liquid and surfaces

Six different liquids, both Newtonian and non-Newtonian and three surfaces were prepared to perform this experimental investigation. Liquid shear viscosities were measured with Bohlin CS 10 Rheometer with cone-plate arrangement and it ranged from 1mPa.s to 340mPa.s. The impingement surfaces were prepared carefully to eliminate the effects of surface roughness on splash characteristics. Static contact angle (Table 2) of liquids with impingement surfaces were measured with a high-resolution camera and image processing software.

Table 8 Static contact angles in degrees

Liquids	Glass	Steel	Teflon
Water	17.5	60	103.5
Water-15% + Glycerin-85%	20.3	58	97
Water-25% + Glycerin-75%	23.8	55.7	100.5
Propylene Glycol (PG)	13.5	63.5	101.8
Silica-10% + PG-90%	19.5	63	102
Silica-14% + PG-86%	18	64	100

A.2 Results and discussion

Experiments were carried out to study effects of static contact angle on the splash threshold of a jet impinging on a moving surface. The jet and projectile velocity and liquid shear viscosity were selected carefully so that Reynolds number is in the vicinity of the splash threshold. Figures 37-A, 37-B and 37-C show deposition of water – 15 % + glycerin – 85% jet impinging on glass, steel and Teflon surfaces respectively. Similarly Figures 37-D, 37-E and 37-F show splash of the same liquid on these surfaces. The Reynolds number of this experiment ranged from 350-450 and Weber number ranged from 1000-1200.

The contact angles for this liquid on the given surfaces vary from 10 to 101 (Table 2). In contrast with results from droplet impact on a dry surface, where contact angle is an important parameter in determining droplet spreading, the results for jet impingement show that splash or deposition is independent of the type of impingement surface. This experiment has been performed for several other liquids (mentioned in Table 8) and the results show the same behavior i.e. splash or deposition is independent from wettability of the surface at these Weber numbers.

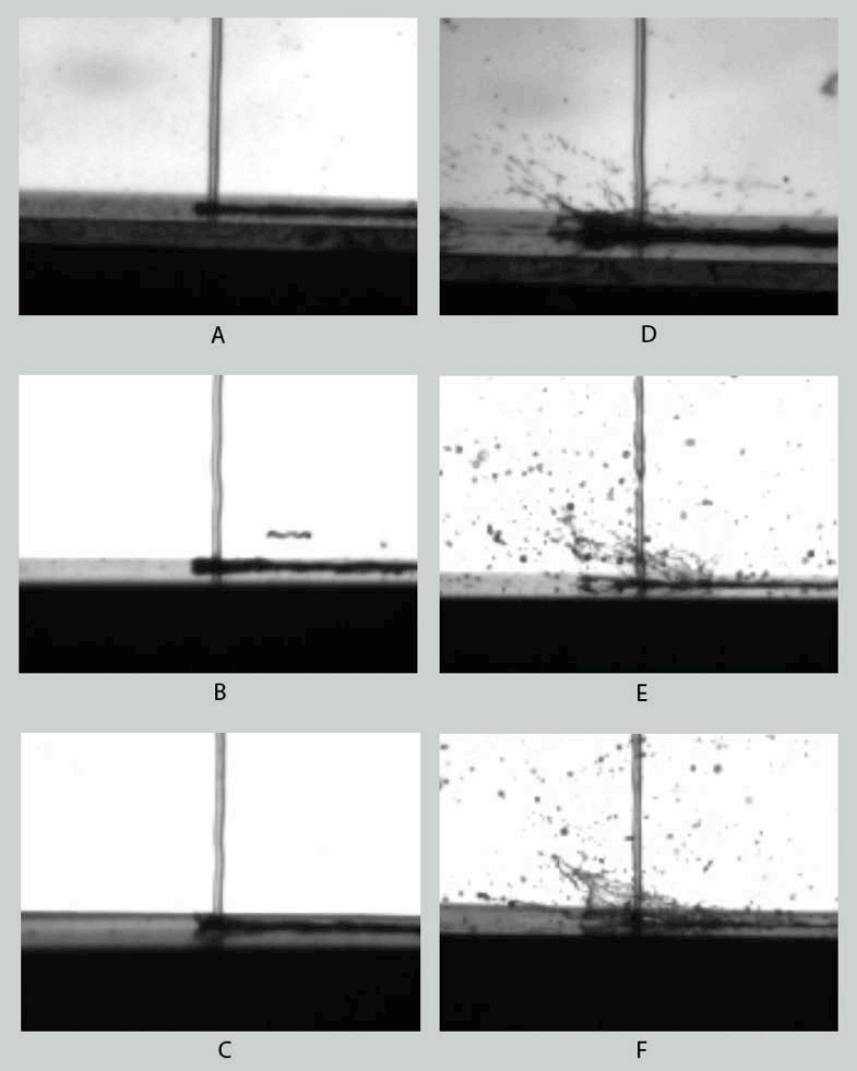

Figure 37 (A-C) Deposition and (D-E) splash of an elastic jet on a moving surface traveling from left to right with 5.3 m/s. Jet speed in left column (A-C) is 11.3 m/s, before splash threshold and in right column (D-F) is 13.5 m/s, after splash threshold.

A.3 Conclusions

For investigation of static contact angle six liquid samples and three surfaces were prepared. Both splash and deposition happened on all three surfaces simultaneously regardless of their contact angles. In other words, when deposition happened on the glass surface it happened on both steel and Teflon as well, and the same results appeared when splash happened on glass surface. The results were repeatable with different test liquids.

B - Experiments with pure shear thinning fluids

Experiments were also conducted with pure shear thinning liquids to study effects of consistency constant on the splash threshold of jet impingement. The water-xanthan gum solutions were used for these studies. The water-xanthan gum solutions are non-Newtonian shear thinning liquids with very small yield stress. Although these liquids show yield stress due to its smaller value it can be considered as pure shear thinning liquids.

The table blow shows the rheological properties of water-xanthan gum solutions.

Table 9 Rheological properties of water-xanthan gum solutions

Percentage of xanthan gum	Yield stress (Pa)	Consistency constant	Power-law index
0.1	1.26	0.026	0.81
0.2	2.16	0.055	0.77
0.5	5.51	0.220	0.65
0.75	7.9	0.422	0.60
1.0	12.54	0.78	0.58
1.5	17.65	1.23	0.55

B.1 Mass flow rate experiments

Mass flow rate experiments were conducted to obtain the liquid jet velocities corresponding to nozzle pressure. Experimental setups used in Chapter 2 were also used here. The liquid jet was created using 648 micron nozzle.

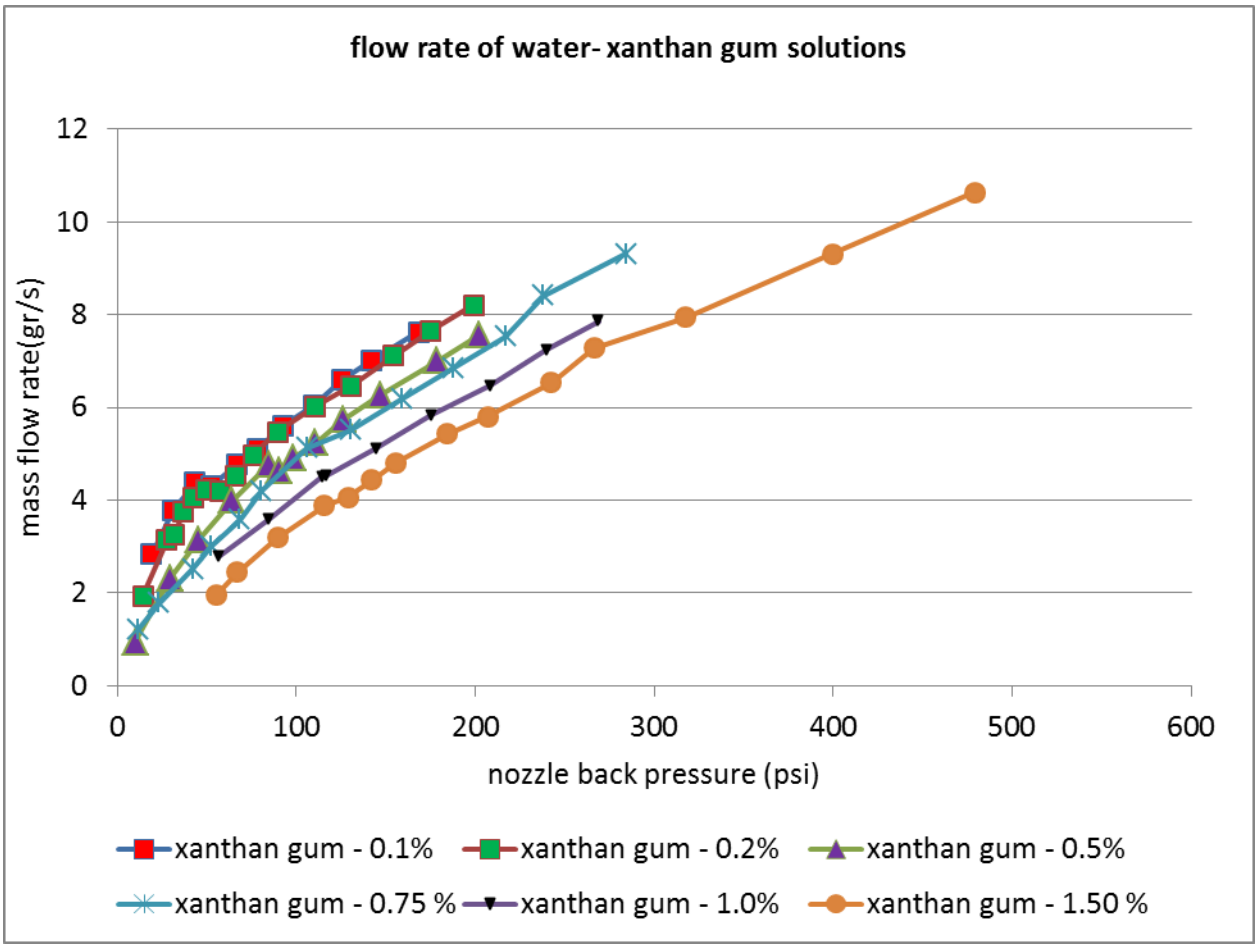

Figure 38 Mass flow rates of water-xanthan gum solutions

Figure 38 clearly shows that with 648 micron nozzle the mass flow liquids with smaller consistency constant (0.1 and 0.2 percent) show cavitation between 4 to 6 gr/s. Similar results with other non-Newtonian liquids have also been reported in Chapter 2.

B.2 Splash-deposition results

The table below shows the splash thresholds of the water-xanthan gum solutions. Several experiments were carried out for individual liquids starting from low jet and surface speeds with continuous increase in small increments. Once splash of the liquid jet started we report it as splash threshold here.

Table 10 Splash thresholds for water-xanthan gum solutions

Percentage of xanthan gum	Jet velocity (m/s)	Surface velocity (m/s)	Resultant velocity (m/s)
0.1	10.8	6.49	12.6
0.2	10.3	6.91	12.4
0.5	18.7	5.70	19.5
0.75	20.3	6.59	21.3
1.0	26.3	6.30	27.1
1.5	31	6.20	31.8